



THE UNIVERSITY *of* EDINBURGH

## Edinburgh Research Explorer

# Interactions of CO<sub>2</sub> with Formation Waters, Oil and Minerals and CO<sub>2</sub> storage at the Weyburn IEA EOR site, Saskatchewan, Canada

### Citation for published version:

Hutcheon, I, Shevalier, M, Durocher, K, Bloch, J, Johnson, G, Nightingale, M & Mayer, B 2016, 'Interactions of CO<sub>2</sub> with Formation Waters, Oil and Minerals and CO<sub>2</sub> storage at the Weyburn IEA EOR site, Saskatchewan, Canada', *International Journal of Greenhouse Gas Control*.  
<https://doi.org/10.1016/j.ijggc.2016.08.004>

### Digital Object Identifier (DOI):

[10.1016/j.ijggc.2016.08.004](https://doi.org/10.1016/j.ijggc.2016.08.004)

### Link:

[Link to publication record in Edinburgh Research Explorer](#)

### Document Version:

Peer reviewed version

### Published In:

International Journal of Greenhouse Gas Control

### Publisher Rights Statement:

© 2016 Elsevier Ltd. All rights reserved.

### General rights

Copyright for the publications made accessible via the Edinburgh Research Explorer is retained by the author(s) and / or other copyright owners and it is a condition of accessing these publications that users recognise and abide by the legal requirements associated with these rights.

### Take down policy

The University of Edinburgh has made every reasonable effort to ensure that Edinburgh Research Explorer content complies with UK legislation. If you believe that the public display of this file breaches copyright please contact [openaccess@ed.ac.uk](mailto:openaccess@ed.ac.uk) providing details, and we will remove access to the work immediately and investigate your claim.



## **Interactions of CO<sub>2</sub> with Formation Waters, Oil and Minerals and CO<sub>2</sub> storage at the Weyburn IEA EOR site, Saskatchewan, Canada**

**Ian Hutcheon<sup>1</sup>, Maurice Shevalier<sup>1</sup>, Kyle Durocher<sup>1</sup>, John Bloch<sup>2</sup>, Gareth, Johnson<sup>3</sup>, Michael Nightingale<sup>1</sup> and Bernhard Mayer<sup>1</sup>**

<sup>1</sup>Applied Geochemistry Group, Department of Geoscience, University of Calgary, Calgary, Alberta, Canada, T2N 1N4

<sup>2</sup>Guadalupita, New Mexico, USA

<sup>3</sup>School of Geosciences, University of Edinburgh, Edinburgh, United Kingdom, EH9 3FE

### **Abstract**

The Weyburn oil field in Saskatchewan, Canada, is hosted in Mississippian carbonates and has been subject to injection of CO<sub>2</sub> since 2000. A detailed mineralogy study was completed as the basis for modeling of mineral storage of injected CO<sub>2</sub>. Combining the mineralogy with kinetic reaction path models and water chemistry allows estimates of mineral storage of CO<sub>2</sub> over 50 years of injection. These results, combined with estimates of pore volume, solubility of CO<sub>2</sub> in oil and saline formation waters, and the initial and final pore volume saturation with respect to oil, saline water and gas/supercritical fluid allow an estimate of CO<sub>2</sub> stored in saline water, oil and minerals over 50 years of CO<sub>2</sub> injection. Most injected CO<sub>2</sub> is stored in oil ( $6.5 \cdot 10^6$  to  $1.3 \cdot 10^7$  tonnes), followed closely by storage in supercritical CO<sub>2</sub> ( $7.2 \cdot 10^6$  tonnes) with saline formation water ( $1.5 - 2 \cdot 10^6$  tonnes) and mineral storage ( $2 - 6 \cdot 10^5$  tonnes) being the smallest sinks. If the mineral dawsonite forms, as modeling suggests, the majority of CO<sub>2</sub> dissolved in oil and saline formation water will be redistributed into minerals over a period of approximately 5000 years. The composition of produced fluids from a baseline sampling program, when compared to produced fluids taken three years after injection commenced, suggest that dawsonite is increasingly stable as pH decreases due to CO<sub>2</sub> injection. The results suggest that hydrocarbon reservoirs that contain low gravity oil and little or no initial gas saturation prior to CO<sub>2</sub> injection, may store the majority of injected CO<sub>2</sub> solubilized in oil, making such reservoirs the preferred targets for combined enhanced oil recovery-CO<sub>2</sub> storage projects.

## 1 **1. Introduction**

2 Carbon capture and geological storage (CCS) is a promising technology for reducing CO<sub>2</sub>  
3 emissions into the atmosphere from fossil fuel intensive industries and energy production  
4 (Intergovernmental Panel on Climate Change (IPCC), 2005). There are over 200 enhanced oil  
5 recovery CO<sub>2</sub> injection projects in the United States and six in Canada as of 2015 (Verma,  
6 2015). This technology has been piloted at various sites world-wide for more than 15 years and  
7 several full-scale storage projects have been established. As of December 2015, the  
8 Massachusetts Institute of Technology Carbon Capture and Sequestration technologies world-  
9 wide on-line database (sequestration.mit.edu) shows 22 power plant CCS projects, 33 non-  
10 power plant CCS projects, 9 commercial Enhanced Oil Recovery (EOR) projects, and 25 pilot  
11 CCS projects ranging from a few tonnes, to millions of tonnes, per year of injected CO<sub>2</sub>. For all  
12 CO<sub>2</sub> injection sites, it is highly desirable to monitor the CO<sub>2</sub> plume distribution within the target  
13 reservoir and to verify the nature and amount of CO<sub>2</sub> storage in the reservoir, so as to  
14 demonstrate the conformance and safety of these operations.

15

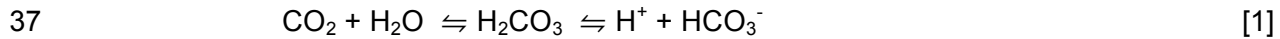
16 Storage of CO<sub>2</sub> in geological reservoirs may occur as supercritical fluid underneath the caprock,  
17 as residual trapping in pore spaces, solubility trapping in formation water, or mineral trapping.  
18 As outlined and predicted by the IPCC (2005), storage as supercritical fluid and via residual  
19 trapping are expected to be dominant in the early years of CO<sub>2</sub> storage projects. Solubility  
20 trapping in the formation waters is assumed to steadily increase in the medium term (e.g.  
21 decades). Mineral trapping of injected CO<sub>2</sub> has been suggested as a long-term process that  
22 may fix injected CO<sub>2</sub> on timelines of hundreds to thousands of years (IPCC, 2005), although  
23 faster rates of mineral trapping have been observed under favorable circumstances (Matter et  
24 al., 2016). Over the last few years, sufficient monitoring data have emerged from various CO<sub>2</sub>  
25 storage reservoirs to allow testing of the efficiency of CO<sub>2</sub> storage mechanisms and the  
26 associated time lines that are dependent on the reservoir.

27

28 The relative contributions of the various CO<sub>2</sub> storage mechanisms and their temporal evolution  
29 are critically dependent on whether CO<sub>2</sub> is injected into saline aquifers or whether CO<sub>2</sub> is used  
30 for enhanced oil recovery in mature oil fields such as Weyburn. Furthermore, the reservoir  
31 geology and mineralogy is of critical importance for assessing the reactions and reaction rates  
32 involved in geological CO<sub>2</sub> storage and sequestration (Gunter et al., 2004). Solubility trapping of  
33 injected CO<sub>2</sub> as in reaction [1] occurs as dissolved CO<sub>2</sub> in saline formation water as H<sub>2</sub>CO<sub>3</sub>,  
34 HCO<sub>3</sub><sup>-</sup>, and CO<sub>3</sub><sup>2-</sup>, depending on salinity and chemistry of the water and pressure and

35 temperature of the reservoir (Duan and Sun, 2003).

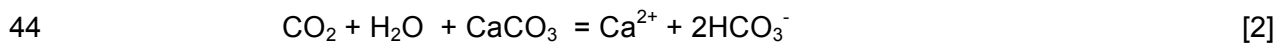
36



38

39 Ionic trapping takes place when the injected CO<sub>2</sub> lowers the pH of the formation water causing  
40 dissolution of carbonate minerals, such as calcite, as in reaction [2]. Half of the carbon in the  
41 bicarbonate in reaction [2] results from dissolution of CO<sub>2</sub>, the other half from dissolution of  
42 carbonate minerals.

43



45

46 In a three week, single well “push-pull” CO<sub>2</sub> injection test into the contact between a dolerite sill  
47 and metamorphosed siltstones and mudstones, Assayag et al. (2009) observed that dissolution  
48 of carbonate minerals was the dominant mechanism to neutralize H<sub>2</sub>CO<sub>3</sub>, followed by cation  
49 exchange or dissolution of silicate minerals. A similar short-term (3 days) test of CO<sub>2</sub> injection in  
50 the Frio Formation, a fine grained quartz feldspar sandstone with minor amounts of illite,  
51 smectite and calcite showed calcite dissolution as the dominant reaction (Hovorka et al., 2006;  
52 Kharaka et al., 2006). Further sampling over an eight-month period showed increase in  
53 dissolved iron and, potentially increases in dissolved organics. Using the Frio data, a 1-D radial  
54 flow model for reactive transport shows that gas saturation decreases due to dissolution and the  
55 formation of carbonate minerals, with all the injected CO<sub>2</sub> ultimately sequestered as carbonates  
56 (Xu et al., 2010). Using carbon isotope ratios, Mayer et al. (2013) showed movement of injected  
57 CO<sub>2</sub> from injectors to producers, dissolution of CO<sub>2</sub> in reservoir saline waters, and ionic trapping  
58 of injected CO<sub>2</sub> in conjunction with dissolution of carbonate minerals (Shevalier et al., 2013)  
59 over a ten year period at the Weyburn IEA EOR site. In mature oil fields, dissolution of  
60 molecular CO<sub>2</sub> in oil is an additional possible pathway of solubility trapping. Due to the high  
61 solubility of CO<sub>2</sub> in many oils (Mungan 1981), enhanced oil recovery projects using CO<sub>2</sub> are  
62 likely to achieve elevated solubility trapping of CO<sub>2</sub> more rapidly than CO<sub>2</sub> storage projects in  
63 saline aquifers. At Weyburn, Perez et al. (2006) conclude that significant dissolution of CO<sub>2</sub> in oil  
64 took place over a three-year period.

65

66 The extent of mineral trapping is equally dependant on the type of reservoir in which CO<sub>2</sub> is  
67 injected. Carbonate reservoirs, typically containing Ca, Mg, and Fe-bearing carbonates are  
68 considered to have low mineral trapping potential as injected CO<sub>2</sub> results in low pH, causing

69 carbonate minerals to dissolve. In contrast, siliciclastic minerals may buffer pH (Hutcheon et al.,  
70 1993) and provide additional potential for storage of CO<sub>2</sub> in the mineral and/or aqueous phase  
71 by reactions with aluminous silicate minerals (Gunter et al., 2000). Numerical simulation of  
72 kinetic mineral trapping of CO<sub>2</sub> by Xu et al. (2004) shows a strong dependence on rock type,  
73 with mineral trapping being of the same order of magnitude as dissolution of CO<sub>2</sub> in saline  
74 formation waters. These authors also showed that carbonate accumulation may reduce porosity  
75 and permeability, ultimately affecting fluid flow. Reservoirs containing aluminosilicate mineral  
76 assemblages, including feldspar, mica, or clay minerals, among others, can result in  
77 precipitation of Ca-Mg-Fe carbonate minerals and, potentially, dawsonite (NaAlCO<sub>3</sub>(OH)<sub>2</sub>).  
78 Some studies dispute that dawsonite can form, or persist, during CO<sub>2</sub> injection (Hellevang et al.,  
79 2005, 2011, 2013). Worden (2006) has reported diagenetic dawsonite in the Triassic Lam  
80 Formation, Yemen. Up to 8 % (volume) dawsonite is observed and is interpreted to have formed  
81 between 85-100°C, preceding the growth of ferroan dolomite, and post-dating quartz. Some  
82 dawsonite is observed replacing plagioclase (albite) in perthite (plagioclase-potassium feldspar  
83 intergrowth). Dawsonite is reported as a diagenetic mineral from the Aldebaran Sandstone  
84 (Baker, 1991), Australia and is interpreted to have formed late in the burial history, or possibly at  
85 present. Present day temperatures range from 20-75°C. Dawsonite is also reported as a  
86 diagenetic mineral in Eastern Australia (Baker et al., 1995) and is interpreted as being formed  
87 due to seepage of magmatic CO<sub>2</sub> at temperatures between 30-75°C. Ferrini et al. (2003) report  
88 hydrothermal formation of dawsonite in a mineralogically complex dawsonite-realgar-orpiment  
89 hydrothermal deposit at Koran, Albania. The dawsonite is associated mainly with dolomitic wall  
90 rocks that contain ankerite and subordinate amounts of quartz and clay minerals, rather than the  
91 relatively lower porosity sandstone-shale wall rocks, due to greater porosity of the former.  
92 Irrespective of whether or not dawsonite forms during injection of CO<sub>2</sub>, it appears that  
93 siliciclastic reservoirs are generally more favorable for mineral trapping of injected CO<sub>2</sub> than  
94 carbonate reservoirs, although the latter may also contain some potentially reactive silicate  
95 minerals. Hellevang et al. (2013, and references therein) summarize known natural occurrences  
96 of dawsonite and conclude that extensive formation of dawsonite is usually found in alkaline  
97 environments. Natural environments in China and Yemen with high pCO<sub>2</sub> and circum-neutral pH  
98 do exist and in at least two examples dawsonite has formed from replacement of Na-plagioclase  
99 (albite). Hellevang et al. (2013) also note high CO<sub>2</sub> zones in the North Sea, lacking in Na-  
100 plagioclase, that do not show dawsonite formation, in spite of dissolution of K-feldspar and  
101 calcite, likely resulting from kaolinite forming as K-feldspar dissolves, limiting availability of Al<sup>3+</sup>.

102

103 From the preceding discussion, it follows that each storage reservoir will retain injected CO<sub>2</sub> by  
104 a mixture of different mechanisms and over different timelines. Therefore, CO<sub>2</sub> storage  
105 mechanisms and associated timelines should be determined and predicted for each geological  
106 storage site separately, provided that sufficient information is available on the geology,  
107 mineralogy, fluid geochemistry, reaction rates, porosity, and the distribution of oil, saline water  
108 and gas, in the proposed storage reservoir. One of the major CO<sub>2</sub> storage projects where this is  
109 feasible is the IEA-GHG Weyburn-Midale CO<sub>2</sub> Monitoring and Storage project in Saskatchewan,  
110 Canada.

111 The objective of this paper is to determine the potential storage of CO<sub>2</sub> in individual flow units  
112 within the Midale beds of the Weyburn field in the Phase 1A area (Figure 1). The storage  
113 reservoirs considered for CO<sub>2</sub> are:

- 114 • newly formed minerals
- 115 • ionic species in solution in saline formation water
- 116 • CO<sub>2</sub> dissolved in oil
- 117 • CO<sub>2</sub> in a gas of mixed composition and/or a supercritical phase.

118

## 119 **2. Study Area and Background**

### 120 **2.1 Geological Setting**

121 The Weyburn Oil Field in southeastern Saskatchewan covers an area of 180 km<sup>2</sup> and produces  
122 oil from Mississippian carbonates of the Williston Basin (Burrowes, 2001). The field was  
123 discovered in 1954 and after various stages of primary and secondary production, the owner of  
124 the field (PanCanadian, subsequently EnCana and now Cenovus) began a CO<sub>2</sub> injection project  
125 in 2000 to determine the feasibility of improving oil recovery. An agreement between industry,  
126 government and academia coordinated by the Petroleum Technology Research Centre (based  
127 in Regina, Saskatchewan) and sponsored by the International Energy Agency Greenhouse Gas  
128 (IEA-GHG) Research and Development Program implemented a \$40 million (CAD) international  
129 research project to combine the enhanced recovery effort with a CO<sub>2</sub> storage project at  
130 Weyburn (Wilson and Monea, 2004). The overall objective of the Weyburn Project was to  
131 assess the technical and economic feasibility of CO<sub>2</sub> storage in geological formations, to  
132 develop tools to predict and verify CO<sub>2</sub> storage performance, and to build a set of best practice  
133 guidelines for such projects (Hitchon, 2012). An outline of all the research activities at Weyburn

134 is presented in White et al. (2009). The scope of the IEA GHG Weyburn Monitoring and Storage  
135 Project includes a detailed geological, petrophysical, hydrogeological, geophysical, and  
136 geochemical study of the reservoir, caprock, overburden and surrounding surface and  
137 subsurface region. While significant progress has been made on these objectives, so far a  
138 comprehensive CO<sub>2</sub> storage budget revealing the predominant CO<sub>2</sub> trapping mechanisms in the  
139 Weyburn field has not been provided.

140  
141 Burrowes and Gilboy (2000) presented the geological setting of the Weyburn reservoir, and the  
142 distribution of flow units within the reservoir is described by Burrowes (2001). The Weyburn field  
143 is one of a number of large oilfields that lie along the Mississippian subcrop belt on the northern  
144 extent of the Williston Basin approximately 130 kilometers southeast of Regina, Saskatchewan.  
145 Medium gravity crude oil is produced from the Midale beds of the Mississippian Charles  
146 Formation. The location, stratigraphy and operational factors at Weyburn are presented in  
147 Shevalier et al. (2013). A detailed description of the lithofacies and depositional history of the  
148 Midale in southeastern Saskatchewan in the vicinity of the Weyburn field is presented by Qing  
149 and Nimegeers (2008). Regional hydrogeology and hydrogeochemistry for the Midale Fm., as  
150 well as the overlying Ratcliffe and underlying Frobisher Formations is detailed by Jensen et al.  
151 (2013).

152  
153 A complete description of the stratigraphy and the geological position of the Marly and Vuggy  
154 flow units at Weyburn is given in Shevalier et al. (2013), and the following is a brief summary.  
155 The Weyburn reservoir is comprised of the tight dolomitic Marly zone and the underlying calcitic  
156 more permeable Vuggy Shoal, and less permeable Vuggy Intershoal zones, and is sealed by  
157 the Midale Evaporite anhydrite cap. Cenovus Ltd., the operator of the Weyburn field, has  
158 established a core-based, sequence stratigraphic interpretation of the Midale Marly and Midale  
159 Vuggy units (Figure 2 in Shevalier et al., 2013; Burrowes, 2001). Burrowes (2001) and Burrowes  
160 and Gilboy (2000) list general porosity and permeability estimates for the various flow units. The  
161 Midale Marly is characterized by high porosity (26%), and variable permeability (10 MD). The  
162 Midale Vuggy shoal has lower porosity (15%), but high permeability (50 MD), and the Vuggy  
163 intershoal unit is characterized by low porosity (10%) and low permeability (3 MD). Burrowes  
164 (2001) describes the Midale Vuggy as a heterogeneous calcareous, algal/coated-grain/pisolitic  
165 wackestone, packstone and grainstone with visible fenestral and vuggy porosity. The Marly is  
166 described as microsucrosic dolostone with mud dominant fabric. There is patchy cementation by  
167 calcite, anhydrite and dolomite. An examination of the potential effect of the petrology of the

168 Marly and Vuggy on mineral reactions and storage of CO<sub>2</sub> at Weyburn is presented by Durocher  
169 et al. (2003, 2005).

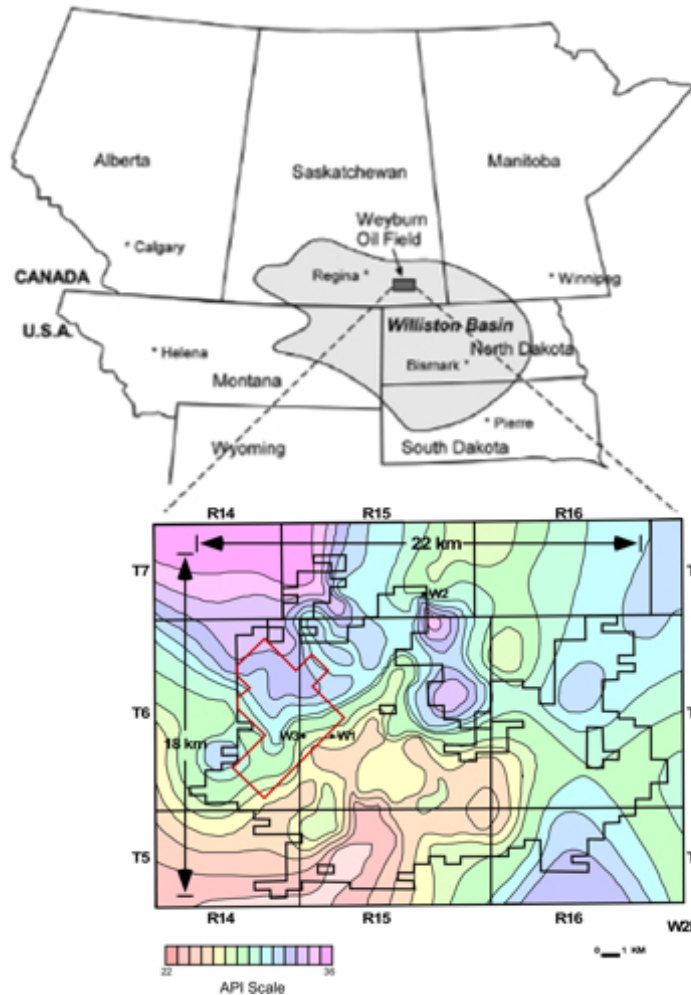
170

## 171 **2.2 CO<sub>2</sub> Flood and Enhanced Oil Recovery**

172

173 Injection of CO<sub>2</sub> improves oil recovery by lowering interfacial tension, swelling the oil, reducing  
174 viscosity and by mobilizing lighter components in the oil (Verma, 2015). Injection of CO<sub>2</sub> started  
175 at Weyburn in the fall of 2000 in the Phase 1A area, in the northwest corner of the Weyburn  
176 field. Early experimental studies outlined the mechanisms of CO<sub>2</sub> enhanced recovery (Holm,  
177 1959). Correlations to determine miscibility of CO<sub>2</sub> with oil show a dependence on oil  
178 composition and density (API gravity) (Holm and Josendal, 1974; Mungan 1981). Oil density  
179 varies widely over the Weyburn field (Figure 1), thus solubility of CO<sub>2</sub> is expected to be variable.  
180 Srivastava and Huang (1997) and Srivastava et al. (2000) have measured the solubility of CO<sub>2</sub>  
181 in Weyburn reservoir oils. Sampling of oil from a single well at Weyburn over a ten year period  
182 shows dissolution of CO<sub>2</sub> in oil up to 38.5 mol percent (Yuo et al., 2013). A preliminary estimate  
183 for the entire Weyburn field suggests potential storage of up to 45.15 MT of CO<sub>2</sub>, comprised of  
184 trapping by solubility (22.65 MT), ionic (0.25 MT) and equilibrium mineral storage (22.25 MT)  
185 mechanisms (Wilson and Monea, 2004). A detailed study of produced fluid compositions by  
186 Shevalier et al. (2013) confirms that CO<sub>2</sub> dissolution in saline water and subsequent reaction  
187 with calcite has taken place over a ten-year period of CO<sub>2</sub> injection at Weyburn. Shevalier et al.  
188 (2013) present the mechanisms and amounts of CO<sub>2</sub> stored in saline formation water by  
189 solubility and ionic trapping at Weyburn in Phase 1A. As of 2012, 22 million tonnes have been  
190 injected over the entire Weyburn field (Petroleum Technology Research Centre, 2014). Injection  
191 data since that date are not presently available.





192  
 193 Figure 1. Location map of the Weyburn field in southern Saskatchewan, Canada. The phase 1A  
 194 area is shown in the shaded area of the inset. The inset map of the Weyburn field is contoured  
 195 for values of oil API gravity. W1, W2 and W3 are the locations of wells with measured solubility  
 196 of CO<sub>2</sub> in oil from Srivastava et al. (2000).

197  
 198 **3. Methodology**

199 One hundred (100) core samples were obtained from the flow units described by Burrowes  
 200 (2001). Cenovus supplied flow unit intervals (personal communication, Geoff Burrowes) and  
 201 samples of drill core were selected to maximize the number of samples obtained from each flow  
 202 unit. Cores were also selected to correlate with wells sampled for the geochemistry fluid/gas  
 203 monitoring program that was conducted at Weyburn (Emberley et al., 2005; Raistrick et al.,  
 204 2006; Shevalier et al., 2013). Five primary analytical methods were utilized: 1. Polished thin  
 205 section examination by petrographic (PM) and scanning electron (SEM) microscopy to obtain  
 206 general textural and mineralogical information. 2. X-Ray Diffraction (XRD) to provide mineral

207 identification and relative proportions. 3. X-Ray Fluorescence (XRF) and Inductively-Coupled  
208 Plasma Mass Spectrometry (ICP-MS) to obtain whole rock major and trace element  
209 composition, 4. Electron Probe Microanalysis (EPMA) for mineral identification and chemistry,  
210 and 5. Linear Programming Normative Analysis (LPNORM: Caritat et al., 1994) to produce  
211 quantitative mineralogy from the analytical results.

212

213 Textural information used to inform simulations was gathered by PM and SEM. XRD results  
214 show only the relative proportions of identifiable minerals, and not the absolute abundances.  
215 LPNORM (de Caritat et al., 1994) was used with XRD chemical analytical data (XRF, ICP-MS)  
216 to quantify the amounts and compositions of mineral phases. Whole rock geochemistry results  
217 are primary input for LPNORM, along with XRD estimates and electron probe microanalytical  
218 (EPMA) results. EPMA was used to identify oxides, sulfides, and clay-sized minerals in thin  
219 section, and to gather quantitative mineral composition data for LPNORM input. The computer  
220 code LPNORM (de Caritat et al., 1994) performs normative analysis from a bulk chemical  
221 analysis and from the composition of contained minerals. The user can specify the list of  
222 minerals and elemental oxides to be considered for normative analysis, and their composition  
223 (mineral formulae or geochemical compositions). LPNORM requires that the XRD data, bulk  
224 rock chemistry and the EPMA analyses of individual mineral grains are consistent with the  
225 calculated mineral mode. This combination of a number of methods, requiring that the total rock  
226 composition be consistent with the mineral modes and compositions, has an additional  
227 constraint (conservation of mass) compared to quantitative XRD analysis (e.g. Omotoso et al.,  
228 2006) alone.

229

230 The volumes of CO<sub>2</sub> stored as minerals, in saline formation water, as gas or supercritical fluid,  
231 and in oil were estimated for each flow unit. This was achieved as follows:

- 232 1. Mineralogical variations in flow units of the Phase 1A area of the Weyburn oilfield were  
233 determined.
- 234 2. Equilibrium rock-water reactions resulting from injection of CO<sub>2</sub>, taking account of the  
235 solubility of CO<sub>2</sub> in saline water, were simulated. This step uses initial (pre CO<sub>2</sub> injection)  
236 conditions to provide the starting fluid composition for kinetic models. Simulations of total  
237 CO<sub>2</sub> injected to reach solubility of CO<sub>2</sub> in saline water identified potential mineralogical  
238 storage mechanisms and an estimate of maximum storage by mineral reactions.
- 239 3. Kinetic rock-water reactions during injection of CO<sub>2</sub>, were simulated, taking account of

240 the solubility of CO<sub>2</sub> in saline water. The resulting amount of CO<sub>2</sub> stored is compared to  
241 an equilibrium model. This step approximates the storage by mass transfer, accounting  
242 for rates of dissolution and precipitation of the minerals identified in the previous step.  
243 4. As dawsonite is an important potential contribution to mineral storage, limitations on its  
244 formation and the impact of dawsonite precipitation, or lack thereof, on storage of CO<sub>2</sub>  
245 were examined.  
246 5. The relative amounts of CO<sub>2</sub> present stored as mineral phases, dissolved in saline  
247 formation water, dissolved in a gas (vapor) phase, and dissolved in oil at the end of CO<sub>2</sub>  
248 injection (after 50 years) are then estimated.

249 The steps involved in deriving the estimated relative amounts are:

- 250 1. The solubility of CO<sub>2</sub> in reservoir saline water at P-T is determined for each flow unit  
251 using two baseline water samples representing the range of TDS.
- 252 2. The reaction of CO<sub>2</sub>, utilizing the formation mineralogy, is simulated using the  
253 REACT module of Geochemists Workbench® to calculate CO<sub>2</sub> storage at equilibrium  
254 due to CO<sub>2</sub> solubility in saline formation water and mineral reactions. The resulting  
255 CO<sub>2</sub> consumption is combined with the pore volume and pore saturation (oil-gas-  
256 saline water ratio) pre and post CO<sub>2</sub> injection of Marly and Vuggy flow units to  
257 determine an estimate of maximum CO<sub>2</sub> storage in saline water and minerals in the  
258 Phase 1A unit.
- 259 3. Kinetic models are evaluated for the same conditions as step 2 to determine the  
260 impact that reaction rates have on the amount of mineral storage.
- 261 4. A final audit of the amount of CO<sub>2</sub> stored is presented to evaluate the relative  
262 importance of SO<sub>2</sub> solubility in saline formation water and oil, the amount of  
263 supercritical CO<sub>2</sub>, and the amount stored by mineral reactions, contrasting  
264 equilibrium and kinetic models.

265  
266 Kinetic reaction path models in REACT use the same parameters as the equilibrium models,  
267 except rate constants (Palandri and Kharaka, 2004) and surface areas are included for the  
268 silicate minerals. The first step in the simulations is to equilibrate the mineralogy with the  
269 respective water, high or low TDS, at reservoir conditions (60°C and 170 bar). The resulting fluid  
270 composition is then used with the mineral amounts and reaction rate expressions to evaluate  
271 how much CO<sub>2</sub> is required to reach saturation in the saline formation water over the assumed

272 50 year injection period. The rates for carbonate minerals and anhydrite are not included in  
273 simulations as they react rapidly compared to the silicates.

274

275 The stability of dawsonite is examined by comparing the equilibrium stability field of dawsonite  
276 to the measured chemistry from produced water and gas samples. The equilibrium stability of  
277 dawsonite relative to albite, analcime, Na-beidellite and kaolinite was calculated using the ACT2  
278 module of Geochemists Workbench®. The fugacity of CO<sub>2</sub> was determined from the baseline  
279 and Monitor 9 produced fluid compositions using the produced gas composition, reservoir  
280 temperature and pressure, and fugacity coefficients from Duan and Sun (2003). The activity of  
281 dissolved silica and the activity ratio of Na<sup>+</sup>/H<sup>+</sup> was calculated using SOLMIN88 (Kharaka et al.,  
282 1988) with the pH (aH<sup>+</sup>) determined at reservoir conditions by the methods outlined in Shevalier  
283 et al (2013).

284

## 285 **4. Analytical Results**

### 286 ***4.1 Mineralogy of Storage Reservoir Flow Units***

287

288 The mineralogy results are too extensive to be presented here, however they are available as  
289 supplemental material. Summary results by flow unit that combine all PM, SEM, XRD, XRF,  
290 ICP-MS, EPM data with the average of LPNORM calculated modes, normalized to 100%, are  
291 presented in Table 1.

Table 1. Average LPNORM Mineralogy for Weyburn Reservoir Samples (93). Normalized to 100 wt %

Unit	samples	Flow Unit	Calcite	Dolomite	Anhydrite	Quartz	K-Feldspar	Plagioclase	Illite	Kaolinite	Anatase	Apatite
Midale Evaporite-Three Fingers Zone	8	ME-TF	0.7	60.0	5.3	16.8	9.1	3.0	4.7	0.0	0.3	0.0
Midale Marly	11	M0	11.7	65.9	6.3	7.4	4.9	1.6	2.2	0.0	0.1	0.0
Midale Marly	4	M1	24.4	47.9	20.2	3.6	2.7	1.0	0.1	0.0	0.1	0.0
Midale Marly	15	M3	21.8	62.7	5.2	4.6	3.5	1.3	0.7	0.2	0.1	0.0
Midale Vuggy	7	V1	82.3	11.6	2.8	1.5	0.9	0.6	0.3	0.0	0.0	0.0
Midale Vuggy	12	V2	89.9	5.0	3.6	0.7	0.3	0.4	0.0	0.0	0.0	0.0
Midale Vuggy	6	V3	76.7	16.1	2.5	2.2	1.5	0.8	0.0	0.0	0.0	0.0
Midale Vuggy	12	V4	77.5	13.3	3.3	2.2	2.0	0.9	0.7	0.1	0.1	0.0
Midale Vuggy	6	V6	68.8	14.6	12.8	1.8	0.5	0.3	0.2	0.9	0.0	0.0
Frobisher Marly	10	FM	4.5	72.7	8.1	6.9	4.4	2.0	1.3	0.0	0.1	0.1
Frobisher Evaporite	2	FE	23.5	15.9	59.1	0.8	0.4	0.3	0.0	0.0	0.0	0.0

292

293

294 The most commonly found minerals include dolomite, calcite and trace amounts of ankerite (in  
 295 Marly units of the Midale and Frobisher), calcite (dominantly in Vuggy units), and anhydrite (all  
 296 units to some degree). Silicate minerals quartz, mica (illite) and K-feldspar are also present, and  
 297 tend to be more common in the Marly flow units. Trace amounts of celestite, illite, and gypsum  
 298 were identified. Although pyrite and fluorite were found in trace amounts in most samples  
 299 (EPMA), these minerals were not easily identifiable in XRD traces due to low abundance. K-  
 300 feldspar was found in virtually all samples using the electron microprobe, but was identified in  
 301 only some reservoir samples using XRD. These observations suggest that XRD mineral  
 302 identification is limited to phases in excess of several volume percent.

303

304 Oxide totals for all samples are highly variable and range between 40 and 90 wt.%. The  
 305 average oxide total is approximately 70%. The high loss on ignition (LOI) may be due to  
 306 bitumen and water. Samples that are dominantly calcite (Vuggy) have CaO contents that  
 307 approach 56 wt.%. Dolomitic samples (Marly) have elevated MgO contents (up to 20 wt.%).

308 Silicate-rich samples (Marly) have higher SiO<sub>2</sub>, Al<sub>2</sub>O<sub>3</sub>, and K<sub>2</sub>O contents (up to 50, 7, and 4  
309 wt.%, respectively), while samples with significant amounts of anhydrite and celestite (Vuggy)  
310 have elevated S, Sr, and Ba values (up to 350,000, 35,000, and 700 ppm, respectively).

311  
312 EPMA images and some observations are shown in representative summary Figures 2 and 3.  
313 Several mineral phases were observable using EPMA that were not observed using microscopic  
314 or XRD examination. The most commonly found trace mineral phases (< 3 vol%) are K-feldspar,  
315 illite, fluorite, and pyrite. Less commonly found minerals (< 1 vol%) include celestite, apatite,  
316 anatase, zircon, hematite, pyrrhotite, and chalcopyrite. Calcite and dolomite from reservoir  
317 samples were near the stoichiometric composition (suggesting ordered dolomite), with minor and  
318 variable amounts of SrO, FeO, and MnO. K-feldspar contained variable amounts of Na<sub>2</sub>O and  
319 CaO, potentially reactive elements during silicate-CO<sub>2</sub> reactions in the presence of pore fluids.  
320 Illite grains were typically smaller than 20 μm in length, and were generally too small to analyze  
321 quantitatively.

### 322 ***Petrography, LPNORM Results and Flow Unit Properties***

323 For the purposes of simulations of the water-rock reactions that take place during injection of  
324 CO<sub>2</sub>, it is necessary to have data on the mineralogy, texture, porosity and pore volume of each  
325 flow unit. Cenovus (G. Burrowes; personal communication) provided the porosity and pore  
326 volume for each of the flow units.

327  
328 The petrography, including thin section and backscattered electron photomicrography, is  
329 combined in the following descriptions of individual flow units. Also, the normative calculations,  
330 along with information that is either used to constrain the LPNORM calculation, or to interpret  
331 the results, are presented. Only representative data for the Midale Marly and Midale Vuggy, the  
332 most volumetrically significant units in the Weyburn Field, are presented here, although all units,  
333 including bounding units above and below the Midale, were examined. In the following  
334 discussion, all mineral modes are presented as weight percent. Carbonate rock classification is  
335 according to Dunham (1962).

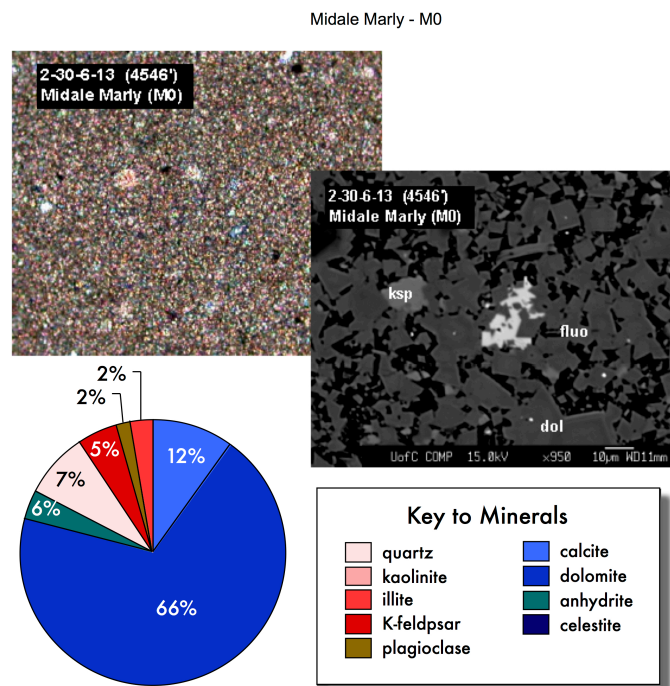
#### 336 337 *Midale Marly*

338 The Midale Marly is a dolomite-dominated series of units (M0, M1, & M3; Burrowes, 2001;  
339 Shevalier et al., 2013, Figure 2) characterized by finely crystalline dolomite (50-65%) and  
340 silicates. Rocks are dominantly mudstone to wackestone (finely crystalline dolomite to

341 biomicrite). Dolomite grains are typically <20 μm in diameter, with some samples displaying  
 342 planar-porphyrrotopic dolomite rhombs up to 100 μm in diameter. All units are either massive  
 343 and structureless, or thinly laminated, with alternating zones of dolomite- and silicate-dominant  
 344 layers. Porosity is generally submicroscopic to pinpoint (<100 μm), subrounded, and clear of  
 345 secondary mineralization. Downward through the stratigraphic section, toward the Midale Vuggy  
 346 units, calcite is more commonly found, with mixed skeletal fragments, anhydrite pore filling, and  
 347 anhydritization. Bitumen is common throughout the Midale Marly.

348  
 349 There are three flow units, M0, M1 and M3 identified in the Midale Marly. The M2 is a low  
 350 porosity calcareous marker (Burrowes, 2001) and is not considered further. Calcite is less  
 351 common than in the Midale Vuggy units, but is still significant (10-25 wt%), with anhydritization  
 352 common only in the M1 flow unit (20 wt%). The Midale Marly has the greatest amount of silicate  
 353 minerals (7.5-16 wt%) of all the reservoir flow units, with quartz being the most common silicate.  
 354 Trace feldspar and illite (approximately 50 wt% of the silicate minerals present) are more  
 355 commonly found within the Marly than the Vuggy shoal and intershoal. LPNORM results  
 356 suggest plagioclase feldspar is dominantly comprised of the albite (Na) component. **Figure 2**  
 357 shows representative views of the M0, which is broadly similar to the M1 and M3 flow units.

358



359

360 Figure 2. Representative petrography and mineral abundance data for the Midale Marly M0 flow  
361 unit. Thin section field of view is 500  $\mu\text{m}$ . Scale bar on the SEM photomicrograph is 10  $\mu\text{m}$ .

362

### 363 *Midale Vuggy*

364 The Midale Vuggy intershoal is a highly variable collection of rock types that range from  
365 microcrystalline calcitic (micrite) mudstone to packstone (intramicrite, dismicrite, and biomicrite  
366 common). V1 flow unit has small to submicroscopic pores (<100  $\mu\text{m}$ ) that are subrounded to  
367 rounded, and largely unfilled although some calcite pore filling is observed. Planar-  
368 porphyrotopic dolomite growth is common, as is anhydritization of micrite. Bitumen layers are  
369 common, most often associated with coarser crystalline silicate-rich layers. Skeletal fragments  
370 are also observed.

371

372 The Midale Vuggy shoal is highly variable in the range of rock types, but also is micritic.  
373 Dominated by wackestone (biomicrite), these units have large, irregularly shaped pores (up to 2  
374 mm diameter), partially filled with calcite, dolomite, and anhydrite. Bioclasts (brachiopod shells,  
375 ooids) are rare to common, as is nodular calcite and celestite. Anhydritization of matrix calcite is  
376 most commonly found at the base of the Vuggy shoal. The lowermost unit immediately overlies  
377 an erosional contact with the Frobisher Marly and Frobisher Evaporite. Compaction features  
378 such as stylolites, elongated pelloidal calcite, and skeletal grains are found in all Vuggy shoal  
379 units.

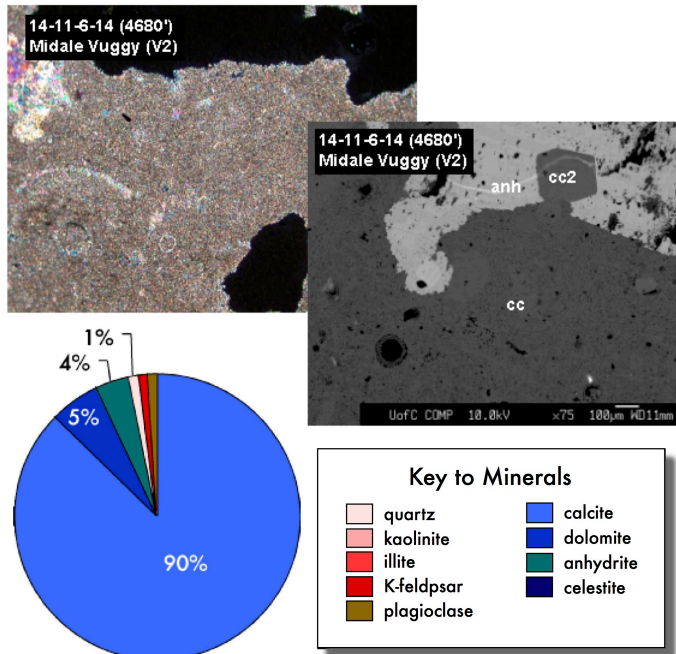
380

381 Five Midale Vuggy flow units were identified by Burrowes (2001), V1, the intershoal unit and the  
382 shoal units V2, V3, V4 and V6. Our results show the Midale Vuggy flow units are dominated by  
383 calcite (70-90%), relatively minor amounts of dolomite (5-15 wt%) and traces of anhydritization  
384 (3-13 wt%). Vuggy flow unit V6, immediately above the Frobisher erosion surface, contains  
385 variable but significant anhydrite (13 wt%). Silicate minerals in the Midale Vuggy are found in  
386 minor to trace amounts (2-15 wt%). Quartz comprises approximately 50 wt% of the silicate  
387 minerals with lesser amounts of plagioclase (albite) and illite. The Midale Vuggy has lower  
388 porosity than the Midale Marly, but the pore structure of the Vuggy has allowed more oil, prior to  
389  $\text{CO}_2$  injection, to be removed proportionally from the Vuggy than the Marly. **Figure 3** shows  
390 representative data for the V2. The V1, V3, V4, and V6 flow units are broadly similar.

391



Midale Vuggy - V2



392

393

394 Figure 3. Representative petrography and mineral abundance data for the Midale Vuggy V2 flow  
 395 unit. Thin section field of view is 500 μm. Scale bar on the SEM photomicrograph is 100 μm.

396

397 The Midale Evaporite Three Fingers Zone represents the top reservoir seal. It has low porosity  
 398 and permeability (not measured) and is comprised dominantly of carbonate minerals and  
 399 anhydrite with significant amounts of K-feldspar, illite and plagioclase. The Midale Marly (M0,  
 400 M1, M3 flow units) is the target for improved oil recovery as it has, prior to CO<sub>2</sub> injection, the  
 401 highest oil saturations. These units have high porosity, approximately 20 volume % on average,  
 402 are dominated by dolomite, and contain 10-20 wt% calcite and minor amounts of quartz with  
 403 traces (less than 5 wt%) of K-feldspar and plagioclase (albite). The M1 and M3 contain the  
 404 greatest pore volume (77% of pore volume) in the Midale Marly. The Midale Vuggy has lower oil  
 405 saturations prior to CO<sub>2</sub> injection, and lower porosity (7-10 volume %). It is dominated by calcite,  
 406 with 5-15 wt% dolomite and minor amounts of quartz. There are lesser amounts of K-feldspar  
 407 (0.4-4.9 wt%) and plagioclase (0.3-2.0 wt%) that LPNORM results show to be albite  
 408 composition. The V1 and V2 flow units account for the majority (60 volume%) of the pore  
 409 volume.

410 **4.2 Geochemistry of Formation Water and Residual Oil**

411 The Weyburn Phase 1A area shows considerable variation in fluid composition within the Midale  
 412 (Emberley et al., 2005), therefore a high total dissolved solids (TDS) and low TDS sample were  
 413 selected from Baseline samples collected in August 2000 at Weyburn (Emberley et al., 2005).  
 414 Well 101/14-30-006-13W2 (47787 mg/l TDS) was selected as the low TDS (referred to as “Lo  
 415 TDS” on subsequent figures) sample with a calculated equivalent salinity of 0.83 M. Well  
 416 141/14-07-006-13W2 (95123 mg/l TDS) was selected as the high TDS sample (referred to as  
 417 “Hi TDS” on subsequent figures) and has a calculated equivalent salinity of 1.67 M. To examine  
 418 the stability of dawsonite, the baseline water and gas compositions are compared to  
 419 compositions from data during monitoring sample trip 9 (Monitor Trip 9, abbreviated M9  
 420 hereafter) collected in September 2003, three years after CO<sub>2</sub> injection began. Fluid  
 421 compositions used in this paper are presented in Table 2.

422

Table 2. Geochemical compositions of produced water from Weyburn Phase 1A.

Baseline Water Compositions - August 2000 (dots represent data not measured)															
DLS LOCATION	Reservoir T	Reservoir P	pH	Alkalinity	S <sup>2-</sup>	Na	K	Ca	Mg	Sr	SiO <sub>2</sub>	Cl	Br	SO <sub>4</sub>	CO <sub>2</sub>
(°C)	(bars)	Downhole	(mg/L)	(ppm)	(mg/L)	(mg/L)	(mg/L)	(mg/L)	(mg/L)	(mg/L)	(mg/L)	(mg/L)	(mg/L)	(mg/L)	(mole %)
101/02-10-006-14W2	52	140	6.61	6.29	578.5	203.7	26070	208.9	1158	306.2	65.19	26.53	44100	3850	5.18
101/02-12-006-14W2	55	195	6.49	6.2	414.6	100.2	18960	382.3	1530	380.2	68.97	23.05	30025	74.0	3.38
101/02-23-006-14W2	57	185	6.81	6.32	605.1	354.3	22560	364.6	1141	337.8	29.18	19.23	33960	46.0	6.00
101/02-24-006-14W2	56	200	6.94	6.43	476.6	88.8	25070	434.5	1318	346.5	31.95	41.31	37555	56.0	3.48
101/02-26-006-14W2	57	195	6.43	6.28	439.0	273.6	20700	488.4	1495	387.7	80.81	40.33	34250	66.5	3.30
101/02-30-006-13W2	58	160	6.85	6.22	389.3	117.8	22510	123.5	1138	365.4	24.47	29.97	34960	59.0	6.47
101/05-36-006-14W2	56	150	6.93	6.44	302.9	25.0	19820	162.9	1049	348.3	27.64	29.27	30225	53.0	3.60
101/08-13-006-14W2	56	202.5	6.73	6.08	407.3	40.7	35860	427.9	1452	399.3	79.38	36.24	51720	72.5	3.45
101/08-19-006-13W2	58	155	7.00	6.21	335.9	13.4	23020	389.7	1195	317.9	29.01	23.90	34320	47.5	3.35
101/08-20-006-13W2	58	150	6.20	5.81	342.9	90.2	27560	365.4	1476	390.9	43.31	32.35	39545	71.0	3.95
101/08-25-006-14W2	56	162.5	6.92	6.44	353.1	45.5	12220	128.4	1008	315.7	42.00	35.62	20635	44.5	3.65
101/08-30-006-13W2	59	145	6.92	6.96	510.9	35.2	21500	218.4	1178	351.1	89.01	27.04	31745	57.5	3.68
101/08-36-006-14W2	56	165	7.30	7.08	264.8	23.5	19940	345.7	1416	373.2	88.50	39.19	30815	60.0	3.67
101/10-17-006-13W2	57	150	6.58	6.12	390.0	19.1	34180	584.9	1504	402.2	39.26	25.24	51200	73.5	3.79
101/11-01-006-14W2	55	170	6.64	5.78	66.3	87.4	28710	400.4	1647	398.1	36.27	23.53	44100	70.5	3.20
101/12-11-006-14W2	54	195	6.47	6.11	537.8	169.3	24570	209.0	1296	368.9	45.65	41.14	37855	67.0	3.90
101/12-18-006-13W2	57	201	7.08	6.29	437.9	60.8	21540	359.6	1138	314.2	23.22	21.37	31645	51.5	3.75
101/12-20-006-13W2	57	160	6.63	5.83	298.6	67.0	30070	558.9	1432	339.7	37.51	24.28	45480	65.5	3.69
101/12-23-006-14W2	58	192.5	6.76	6.38	864.6	686.2	13770	225.2	945	421.1	15.43	52.35	19665	39.5	3.62
101/12-25-006-14W2	55	202.5	6.75	6.7	519.8	284.2	14990	143.9	1122	346.3	31.40	38.64	24150	54.0	3.69
101/12-26-006-14W2	60	155	6.79	6.64	550.4	283.9	22100	193.5	1166	335.5	86.96	19.79	32610	45.5	2.99
101/14-01-006-14W2	54	140	6.34	5.8	493.4	121.6	40850	588.7	1319	411.5	44.38	14.68	60565	95.5	3.10
101/14-02-006-14W2	52	197.5	6.78	6.28	232.7	77.5	29630	611.2	1592	415.1	41.42	23.55	43875	70.5	3.56
101/14-12-006-14W2	55	165	6.81	6.38	419.6	144.5	21720	552.4	1539	382.1	76.28	31.64	36710	69.5	3.69
101/14-14-006-14W2	54	90	6.77	6.25	602.1	44.7	24830	298.1	1402	368.3	30.05	15.96	36570	52.5	3.85
101/14-20-006-13W2	58	206	6.66	5.92	308.3	69.2	25030	400.4	1406	381.6	53.35	29.03	37000	68.5	3.32
101/14-23-006-14W2	60	162.5	6.40	6.3	704.2	133.5	11280	181.4	1110	327.9	62.89	24.13	19650	38.5	3.29
101/14-30-006-13W2	56	150	6.88	6.84	359.3	52.6	16140	107.4	1096	325.5	69.26	31.88	26900	52.0	3.65
121/02-13-006-14W2	58	190	6.68	5.15	398.3	145.6	22890	565.4	1687	399.1	92.56	26.68	35495	66.5	3.46
121/08-17-006-13W2	58	152.5	6.50	5.63	277.0	66.1	35410	710.3	1696	439.0	44.22	37.01	55830	91.0	2.89
121/08-18-006-13W2	55	165	6.45	6.26	395.8	163.2	29740	363.7	1571	385.5	40.71	38.66	44920	69.5	3.24
121/13-18-006-13W2	55	197.5	6.57	6.2	367.0	152.4	30660	395.6	1782	457.1	46.70	15.85	43705	68.0	3.60
121/14-08-006-13W2	52	170	6.88	6.11	391.1	34.6	35000	451.8	1388	374.5	62.02	27.19	47200	73.5	3.26
121/14-13-006-14W2	52	112.5	6.62	6.27	422.0	52.8	27040	294.4	1399	378.1	53.06	19.57	39440	61.0	3.46
141/08-07-006-13W2	58	165	6.57	6.01	358.8	123.6	27730	337.3	1559	390.8	84.07	22.08	42315	74.5	3.95
141/08-12-006-14W2	56	210	6.79	6.35	386.9	49.3	29550	584.1	1615	371.1	39.39	19.75	46375	72.5	3.69
141/08-23-006-14W2	58	155	7.00	6.55	470.7	188.6	24750	404.0	1359	381.5	39.11	25.65	38880	52.0	3.32
141/14-06-006-13W2	56	100	6.84	6.42	710.5	17.2	29730	322.7	1373	425.8	31.76	29.35	51800	96.5	3.04
141/14-07-006-13W2	56	135	6.85	6.09	371.6	138.4	34990	746.1	1552	395.1	45.70	25.63	53400	80.0	3.15
141/14-11-006-14W2	53	115	6.50	5.9	389.3	103.5	29200	512.7	1760	387.0	35.64	22.91	45000	71.0	3.17
141/14-18-006-13W2	55	210	6.31	6.05	437.1	182.9	19920	393.0	1238	363.8	79.68	25.59	32875	56.5	3.60

423

Table 2. Geochemical compositions of produced water from Weyburn Phase 1A.

Baseline Water Compositions - August 2008 (dots represent data not measured)																
DLS LOCATION	Reservoir T	Reservoir P	pH	pH	Alkalinity	S <sup>2-</sup>	Na	K	Ca	Mg	Sr	SiO <sub>2</sub>	Cl	Br	SO <sub>4</sub>	CO <sub>2</sub>
(°C)	(bars)		Downhole	(mg/L)	(ppm)	(mg/L)	(mg/L)	(mg/L)	(mg/L)	(mg/L)	(mg/L)	(mg/L)	(mg/L)	(mg/L)	(mg/L)	(mole %)
10102-10-006-14W2	52	140	6.61	6.29	578.5	203.7	26070	268.9	1158	366.2	65.19	26.53	44100		3850	5.18
10102-12-006-14W2	55	195	6.49	6.2	414.6	100.2	18960	382.3	1530	380.2	68.97	29.05	30025	74.0	3625	3.38
10102-23-006-14W2	57	185	6.81	6.32	605.1	354.3	22560	364.6	1141	337.8	29.18	19.23	33960	46.0	3330	6.00
10102-24-006-14W2	56	200	6.94	6.43	476.6	88.8	25070	434.5	1318	346.5	31.95	41.31	37555	56.0	3485	3.19
10102-26-006-14W2	57	195	6.43	6.28	439.0	273.6	20700	488.4	1495	387.7	80.61	40.33	34250	66.5	3330	4.05
10102-30-006-13W2	58	160	6.85	6.22	388.3	117.8	22510	123.5	1138	365.4	24.47	29.97	34960	59.0	3445	6.47
10105-36-006-14W2	56	150	6.93	6.44	302.9	25.0	19320	162.9	1049	348.3	27.64	29.27	30225	53.0	3605	1.47
10108-13-006-14W2	56	202.5	6.73	6.08	407.3	40.7	35860	427.9	1452	399.3	79.38	36.24	51720	72.5	3455	4.86
10108-19-006-13W2	58	155	7.00	6.21	335.9	13.4	23020	389.7	1195	317.9	29.01	23.90	34320	47.5	3350	4.32
10108-20-006-13W2	58	150	6.20	5.81	342.9	90.2	27580	365.4	1476	390.9	43.31	32.35	39545	71.0	3395	4.08
10108-25-006-14W2	56	162.5	6.92	6.44	351.1	45.5	12220	129.4	1008	315.7	42.00	35.62	29535	44.5	3685	2.92
10108-30-006-13W2	59	145	6.92	6.96	510.9	35.2	21500	218.4	1178	351.1	89.01	27.04	31745	57.5	3685	0.90
10108-36-006-14W2	56	165	7.30	7.08	264.8	23.5	19940	345.7	1416	373.2	88.50	39.19	30815	60.0	3670	0.36
10110-17-006-13W2	57	150	6.58	6.12	390.0	18.1	34160	594.9	1504	402.2	39.26	25.24	51200	73.5	3790	3.12
10111-01-006-14W2	25	170	6.64	5.76	66.3	87.4	28710	400.4	1647	398.1	36.27	23.53	44100	70.5	3205	2.47
10112-11-006-14W2	54	195	6.47	6.11	537.8	169.3	24570	269.0	1296	368.9	45.65	41.14	37855	67.0	3900	6.21
10112-19-006-13W2	57	201	7.08	6.29	437.9	60.8	21540	359.6	1138	314.2	23.22	21.37	31645	51.5	3755	5.59
10112-20-006-13W2	57	160	6.63	5.83	296.6	67.0	30070	558.9	1432	339.7	37.51	24.28	45480	65.5	3690	4.37
10112-23-006-14W2	58	192.5	6.76	6.38	864.6	686.2	13770	225.2	945	421.1	15.43	52.35	19665	39.5	3625	9.40
10112-25-006-14W2	55	202.5	6.75	6.7	519.8	284.2	14990	143.9	1122	346.3	31.40	38.64	24150	54.0	3695	1.28
10112-26-006-14W2	60	155	6.79	6.64	550.4	283.9	22100	193.5	1168	335.5	86.96	19.79	32610	45.5	2995	0.61
10114-01-006-14W2	54	140	6.34	5.8	493.4	121.6	40950	598.7	1319	411.5	44.38	14.68	69565	95.5	3105	4.57
10114-02-006-14W2	52	197.5	6.78	6.28	232.7	77.5	29630	611.2	1592	415.1	41.42	23.55	43875	70.5	3565	2.03
10114-12-006-14W2	55	165	6.81	6.38	419.6	144.5	21720	552.4	1539	382.1	76.28	31.64	36710	69.5	3680	3.62
10114-14-006-14W2	54	90	6.77	6.25	602.1	44.7	24930	298.1	1402	398.3	30.05	15.96	36570	52.5	3385	6.04
10114-20-006-13W2	58	206	6.66	5.52	308.3	69.2	25030	400.4	1406	361.6	53.35	29.03	37000	68.5	3320	4.14
10114-23-006-14W2	60	162.5	6.40	6.3	704.2	133.5	11280	181.4	1110	327.9	62.89	24.13	19650	38.5	3290	5.86
10114-30-006-13W2	56	160	6.88	6.84	359.3	52.6	16140	107.4	1096	325.5	60.26	31.88	26000	52.0	3605	0.87
12102-13-006-14W2	56	190	6.68	6.15	398.3	145.6	23960	568.4	1615	399.1	92.56	29.69	35465	66.5	3465	4.22
12108-17-006-13W2	58	152.5	6.50	5.63	277.0	66.1	35410	710.3	1696	439.0	44.22	37.01	55830	91.0	2895	2.83
12108-18-006-13W2	55	165	6.45	6.26	395.8	168.2	29740	363.7	1571	385.5	40.71	38.66	44920	69.5	3245	3.00
12113-18-006-13W2	55	197.5	6.57	6.2	367.0	152.4	30660	395.6	1782	457.1	46.70	15.85	43705	68.0	3600	3.32
12114-08-006-13W2	52	170	6.88	6.11	391.1	34.6	35000	451.8	1398	374.5	62.02	27.19	47200	73.5	3265	4.47
12114-13-006-14W2	52	112.5	6.62	6.27	422.0	52.8	27040	294.4	1399	378.1	53.06	19.57	39440	61.0	3460	4.16
14108-07-006-13W2	58	165	6.57	6.01	358.8	123.6	27730	337.3	1559	390.8	84.07	22.08	42315	74.5	3595	4.06
14108-12-006-14W2	56	210	6.79	6.35	386.9	49.3	29550	584.1	1615	371.1	39.39	19.75	46375	72.5	3690	4.22
14108-23-006-14W2	58	155	7.00	6.55	470.7	188.6	24750	404.0	1359	361.5	39.11	25.65	36880	52.0	3320	2.48
14114-06-006-13W2	56	100	6.84	6.42	710.5	17.2	29730	322.7	1373	425.8	31.76	29.35	51800	96.5	3045	3.98
14114-07-006-13W2	56	135	6.85	6.09	371.6	138.4	34990	746.1	1552	395.1	45.70	25.63	53400	80.0	3150	4.64
14114-11-006-14W2	53	115	6.50	5.9	389.3	103.5	29200	512.7	1760	387.0	35.64	22.91	49000	71.0	3175	9.69
14114-18-006-13W2	55	210	6.31	6.05	437.1	182.9	19920	393.0	1238	363.8	79.68	25.59	32875	56.5	3650	5.25

424  
425  
426  
427  
428  
429  
430  
431  
432  
433  
434  
435  
436  
437  
438

Srivastava and Huang (1997) and Srivastava et al. (2000) report CO<sub>2</sub> solubility in oil, and oil gravity, an important control on the solubility of CO<sub>2</sub> (Mungan, 1981). API Gravity in the Weyburn field varies from 25°-38° (Srivastava et al., 2000). CO<sub>2</sub> solubility is reported for three wells, W1 (14-17-6-13 W2), W2 (3-11-7-13 W2) and W3 (12-18-6-13 W2 horizontal) in the Phase 1A area. Srivastava et al. (2000) report the initial solubility of CO<sub>2</sub> for their wells W1 and W2 as 70 sm<sup>3</sup>/m<sup>3</sup> (standard cubic meters per cubic meter) and 40 sm<sup>3</sup>/m<sup>3</sup> for well W3 (see Figure 1 for well locations). Note that these solubilities, derived from Srivastava et al. (2000) correspond to pCO<sub>2</sub> of 70 bar, well in excess of the maximum pCO<sub>2</sub> of 18.1 bar observed for the Phase 1A baseline samples. At the initial pre injection conditions of pCO<sub>2</sub> for the low TDS (pCO<sub>2</sub> = 6.3 bar) and high TDS (pCO<sub>2</sub> = 1.3 bar) wells, data from Srivastava et al. (2000) suggest the CO<sub>2</sub> content of the oil is close to 0.0. At the end of injection model conditions of 60°C and 170 bar, the solubility of CO<sub>2</sub> in oil calculated from Srivastava et al. (2000) is 560 sm<sup>3</sup>/m<sup>3</sup> for W1, 640 sm<sup>3</sup>/m<sup>3</sup> for W2 and 330 sm<sup>3</sup>/m<sup>3</sup> for W3. A similar calculation using the ending pCO<sub>2</sub> after 50 years of injection and solubility in oil gives the ending amount of CO<sub>2</sub> stored in oil. The

439 difference between starting and ending amounts represents additional CO<sub>2</sub> storage per unit  
440 volume of oil at the end of injection.

## 441 **5. Estimating CO<sub>2</sub> Storage Budgets in the Weyburn Reservoir**

442  
443 There are four main ways in which injected CO<sub>2</sub> can be stored in the Weyburn oil field:

- 444 1. In saline formation water as dissolved species
- 445 2. As minerals, primarily carbonates, including dawsonite
- 446 3. In oil, as a dissolved species
- 447 4. As supercritical CO<sub>2</sub>

448  
449 We combined the analytical data reported in section 4 with geochemical modeling to assess  
450 which mechanisms contribute to storage of injected CO<sub>2</sub> in the Weyburn reservoir, and to what  
451 extent.

452  
453 Although the Weyburn reservoir is dominantly calcite, dolomite and anhydrite, significant  
454 concentrations (1-5 wt%) of potentially reactive silicate minerals are present and may assist in  
455 CO<sub>2</sub> storage. Reaction of CO<sub>2</sub>-charged fluid with silicate mineral assemblages may allow  
456 trapping of additional CO<sub>2</sub>, especially if reservoir containment is compromised, because CO<sub>2</sub>  
457 can be trapped as carbonate minerals. Equilibrium models are examined first to determine the  
458 sensitivity of CO<sub>2</sub> storage to variations in mineralogy and fluid composition, to suggest potential  
459 reacting phases for kinetic models, and to provide a starting point for kinetic models. Kinetic  
460 models are then examined to approximate the timing of various reactions and to contrast with  
461 equilibrium models employed in the Wilson and Monea (2004) estimates of mineral storage  
462 (45.14 MT). Various poorly known parameters, including mineral surface areas and dissolution  
463 and precipitation rates, can have a significant effect on estimated reaction times. However, the  
464 relative timing of reactions at least qualitatively indicates the reactions that dominate at various  
465 stages of CO<sub>2</sub> storage. One published model of the Weyburn project indicates that dawsonite  
466 forms within a year (Cantucci et al., 2009) and also suggests that K-feldspar dissolves and  
467 subsequently precipitates, along with muscovite and albite, within the first 14 years. They note  
468 that in their simulations after 100 years, the silicates have not achieved equilibrium.

### 469 **5.1 Geochemical Simulations of Mineral-Saline water-CO<sub>2</sub> Interaction**

470 The objective of equilibrium geochemical simulations is to show the relative impact of water  
471 composition and potential reactions that may dissolve or precipitate different mineral phases,

472 not to provide a timeline or to quantify storage. Previous estimates of mineral storage at  
473 Weyburn (Wilson and Monea, 2004) using equilibrium models probably greatly overestimate  
474 actual mineral storage of injected CO<sub>2</sub>. The amount of additional CO<sub>2</sub> stored as minerals and  
475 dissolved in saline formation water is therefore first modeled as though a slug of CO<sub>2</sub> is added  
476 stepwise and reacts with the water and minerals, either first as an equilibrium and subsequently  
477 as a kinetic model. The difference between the baseline amount of CO<sub>2</sub> in the saline water and  
478 the final amount produced as minerals, as ionic species, and as dissolved CO<sub>2</sub> is considered to  
479 be additional stored CO<sub>2</sub>. During this stage of modeling, which covers the injection period (50  
480 years), pure supercritical CO<sub>2</sub> is available to the mineral-saline water system.

481  
482 At Weyburn the temperature and pressure are variable, but an average of 170 bars (1700 KPa)  
483 and 60°C is representative. The initial state of the rock-water system was set by equilibrating  
484 minerals (Muscovite:Al, Dolomite:Mg, K-feldspar:K, Calcite:pH, Anhydrite:SO<sub>4</sub>, Albite:SiO<sub>2</sub>) with  
485 water representative of baseline conditions as outlined previously.

486

**Table 3. Rate Constants and Modelling Parameters**

<b>"Acid" rate</b>			<b>Specific Surf Area (m<sup>2</sup>/g)</b>		<b>Reference</b>
<b>Mineral</b>	<b>log k (mol/m<sup>2</sup>•s)</b>	<b>n1</b>	<b>Marly</b>	<b>Vuggy</b>	
K-feldspar	-10.06	0.5	0.175	0.175	Palandri & Kharaka
Calcite	-0.3		0.034	0.015	Palandri & Kharaka
Dol-dis	-3.19	0.5	0.105	0.014	Palandri & Kharaka
Kaolinite	-11.31	0.777	2.317	0.015	Palandri & Kharaka
Montmorillonite	-12.71				Palandri & Kharaka
Smectite	-10.98				Palandri & Kharaka
Albite	-10.16	0.457			Palandri & Kharaka
Anhydrite	-3.19		0.1	0.1	Cantucci
Dawsonite		0.982	0.14	0.14	Hellevang et al. (2010)
Quartz	-13.4				Palandri & Kharaka
Am Silica	-12.23				Palandri & Kharaka

<b>Neutral Rate</b>		<b>Specific Surf Area (m<sup>2</sup>/g)</b>		<b>Reference</b>
<b>Mineral</b>	<b>log k (mol/m<sup>2</sup>•s)</b>	<b>Marly</b>	<b>Vuggy</b>	
K-feldspar	-12.41	0.175	0.175	Palandri & Kharaka
Calcite		0.034	0.015	Palandri & Kharaka
Dol-dis	-3.19	0.105	0.014	Palandri & Kharaka
Kaolinite	-13.18	2.317	0.015	Palandri & Kharaka
Montmorillonite	-14.41			Palandri & Kharaka
Smectite	-12.78			Palandri & Kharaka
Albite	-12.56			Palandri & Kharaka
Dawsonite		0.14	0.14	Hellevang et al. (2010)
Quartz	-13.40			Palandri & Kharaka
Am Silica	-12.23			Palandri & Kharaka

487

488 Kinetic and equilibrium reaction path models were set up according to the mineralogy based on

489 the average of the LPNORM mineral modes for Vuggy and Marly flow units. The solubility of

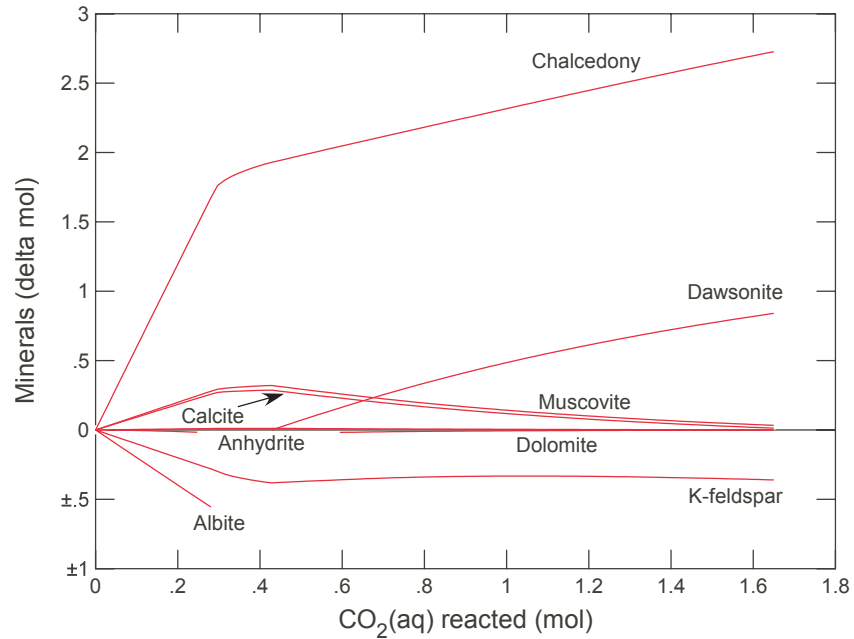
490 CO<sub>2</sub> was calculated (Duan and Sun, 2003) to be 0.985 mol/Kg (low TDS) at 60°C, 170 bar and  
491 0.83 M NaCl and 0.841 mol/Kg (high TDS) at 1.67 M NaCl. In the simulations, CO<sub>2</sub> is added in a  
492 reaction path calculation until the calculated solubility of CO<sub>2</sub> is reached. This represents the  
493 point at which CO<sub>2</sub> no longer will dissolve in the aqueous phase and further addition of CO<sub>2</sub>  
494 must be present in a separate gas or supercritical phase. Plagioclase, K-feldspar and Illite (as  
495 muscovite), included in the reaction path calculation, are present in the samples. The amount of  
496 CO<sub>2</sub> required to reach the solubility value includes CO<sub>2</sub> dissolved in saline water and CO<sub>2</sub> stored  
497 in minerals. Examination of LPNORM results shows that plagioclase is either 100% albite  
498 component, or is dominated by albite (Na plagioclase), therefore no anorthite (Ca component) is  
499 initially present in the simulation, limiting the formation of calcite due to reaction of anorthite.  
500 However, dawsonite (NaAlCO<sub>3</sub>(OH)<sub>2</sub>) could potentially form, either from dissolution of albite, or  
501 from reaction with Na<sup>+</sup> derived from the saline formation water. The water-rock ratio is required  
502 for reaction path models and was determined using LPNORM mineral amounts for each flow  
503 unit, the density of the high and low TDS formation water, and the fraction of the porosity that is  
504 water saturated.

505

#### 506 5.1.1 Equilibrium Reaction Model

507 Representative equilibrium reaction path results for the Marly (M0) are shown in **Figure 4**.  
508 Results for the Vuggy flow units are similar in terms of the reactions, although amounts of  
509 minerals formed and dissolved are different. In the simulations, aluminous silicates are present  
510 in all samples in small amounts (1-5 wt %) and are consumed rapidly as CO<sub>2</sub> is added. Calcite  
511 and dolomite amounts are little affected and a small amount of anhydrite is dissolved, reflected  
512 by an increase in sulfate concentrations in saline water. A small amount of calcite is precipitated  
513 due to the Ca<sup>2+</sup> produced by dissolution of anhydrite. K-feldspar is dissolved throughout the  
514 reaction path, producing muscovite (proxy for illite). Compositions of produced water, discussed  
515 later, suggest that chalcedony is the likely silica polymorph, rather than quartz. Dawsonite (Na-  
516 Al carbonate) is produced initially from Na<sup>+</sup> and Al<sup>3+</sup> derived from albite dissolution and, once  
517 albite is consumed, from Na<sup>+</sup> in the saline water. The pH decreases from 6.6 to 4.7 over the  
518 course of the simulation. The main limiting factor for consumption of CO<sub>2</sub> due to mineral  
519 reactions is the amount of dawsonite that forms, which in turn is limited by the amount of Na<sup>+</sup>  
520 and Al<sup>3+</sup> available, either in the saline formation water or by dissolution of albite. The dissolution  
521 of albite is limited by the kinetics, and the rate of this process is considered in the next section.  
522 Equilibrium is unlikely to be reached within decades, therefore to evaluate the time frame of CO<sub>2</sub>

523 storage, reaction rates (kinetic simulations) are addressed after the equilibrium condition is  
 524 considered.  
 525



526  
 527 Figure 4. Equilibrium reaction path simulation of addition of CO<sub>2</sub> to M0 flow unit at 60°C and 1  
 528 bar.

529  
 530 5.1.2 Kinetic Reaction Model

531 The kinetic reaction model is based on the equation:

$$r = A_s k_+ \left(1 - \frac{Q}{K}\right)$$

532  
 533 where  $r$  is the reaction rate,  $A_s$  is the mineral surface area,  $k_+$  is the dissolution rate constant,  $Q$   
 534 is the activity product and  $K$  is the equilibrium constant for the dissolution reaction. This rate law  
 535 is based on transition state theory (Lasaga, 1984). The temperature dependence of the rate  
 536 constant is based on the Arrhenius equation (Lasaga, 1984; Steefel and Lasaga, 1994).

537  
 538 Shevalier et al. (2013) showed that over a ten-year period at Weyburn, calcite saturation index  
 539 calculations for produced water show calcite to be near equilibrium, although due to large  
 540 variations in CO<sub>2</sub> injection volumes and rates, the variations in saturation states are large.  
 541 Dolomite dissolution is expected from the models presented here, therefore the precipitation of  
 542 dolomite, which is known to be slow, was not considered. Mineral surface areas strongly



543 influence overall reaction rates. For silicate minerals in the Marly and Vuggy core samples, the  
544 surface area was calculated from the average observed grain size in SEM and TS and using the  
545 surface area (A) formulae for either a prism ( $A = 2ab + 2bc + 2ac$ ) or a cube ( $A = 6a^2$ ) as  
546 appropriate from the mineral morphology. The surface areas, and therefore the reaction rates,  
547 are certainly overestimates as the entire surface is not available to react with fluids. As the  
548 minerals present dissolve or precipitate, surface area changes and these changes are  
549 calculated within REACT. Further, experiments by Yang et al. (2008) for Weyburn saline water  
550 suggest the CO<sub>2</sub> saturated formation water has intermediate wettability. In other words the  
551 surface of the rock is likely to be partly oil-wet, further reducing the mineral surface area  
552 available for reaction and decreasing the overall extent of reaction.

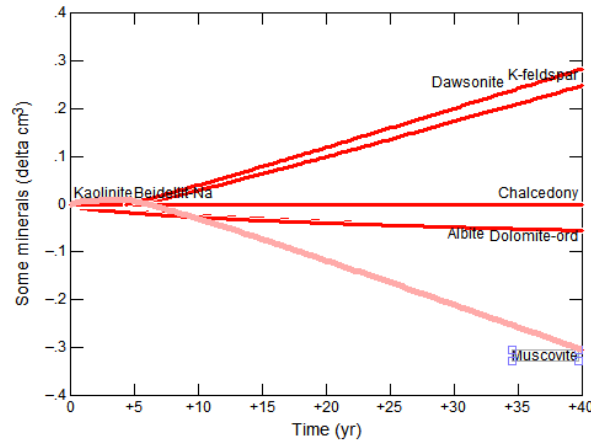
553

554 The rate data for dawsonite suggest that it should form rapidly (within years). However  
555 Hellevang et al. (2011, 2013) suggest that dawsonite, in spite of being present in theoretical  
556 calculations, may not form, or may not persist. Dissolution rates for dawsonite are from  
557 Hellevang et al., (2010), and the rates presented there are more rapid than those reported in  
558 Hellevang et al. (2005) and Palandri and Kharaka (2004). At Weyburn, plagioclase is dominated  
559 by the Na component, albite and, based on the natural analogues described in the introduction,  
560 it is feasible that dawsonite may precipitate as albite is dissolved.

561

562 Figure 5 shows typical results of a kinetic simulation for the M0 flow unit and high TDS water.  
563 The parameters used in the simulations are shown in Table 3. The results, in terms of CO<sub>2</sub>  
564 amounts in various phases, are presented in a later section. Due to the very slow dissolution  
565 rate of albite, which provides the essential constituents to form dawsonite (Na<sup>+</sup> and Al<sup>3+</sup>), the  
566 differences in amounts of albite have limited impact on the total storage of CO<sub>2</sub>. As reaction  
567 rates and surface areas for the minerals involved are not well known, the surface areas and  
568 reaction rates were increased by an order of magnitude, but this causes little or no change in  
569 the amount of reaction and thus the amount of CO<sub>2</sub> required to reach saturation in the saline  
570 formation water. Figure 5 shows precipitating minerals as positive amounts and dissolving  
571 minerals as negative amounts. Initially, muscovite (proxy for illite) dissolves, precipitating K-  
572 feldspar. The simulations show that 31 cm<sup>3</sup> of dawsonite, per Kg of water, forms at the end of 50  
573 years. Chalcedony and kaolinite also precipitate, in amounts less than 5 cm<sup>3</sup> over the entire  
574 simulation. To place the amounts of minerals in perspective, for 1 Kg of water at the porosity of  
575 the M0 flow unit, there is 9813 cm<sup>3</sup> of rock. The 31 cm<sup>3</sup> of dawsonite formed is miniscule in this  
576 context, and were post-CO<sub>2</sub> injection core examined after 50 years, the amounts of minerals

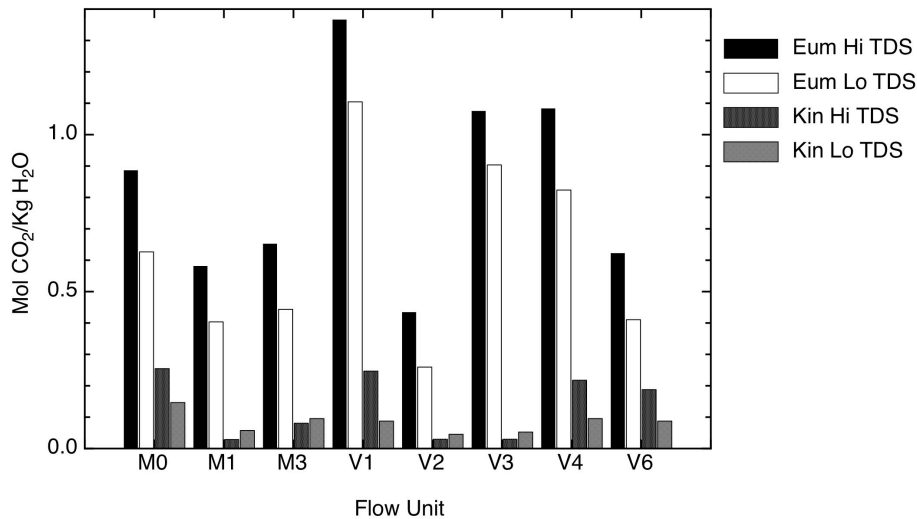
577 precipitated and dissolved would likely be undetectable, especially in the context of the  
578 observed natural variations in mineral amounts.  
579



580  
581  
582 Figure 5. Kinetic reaction path simulation of addition of CO<sub>2</sub> to M0 flow unit at 60°C and 1 bar.

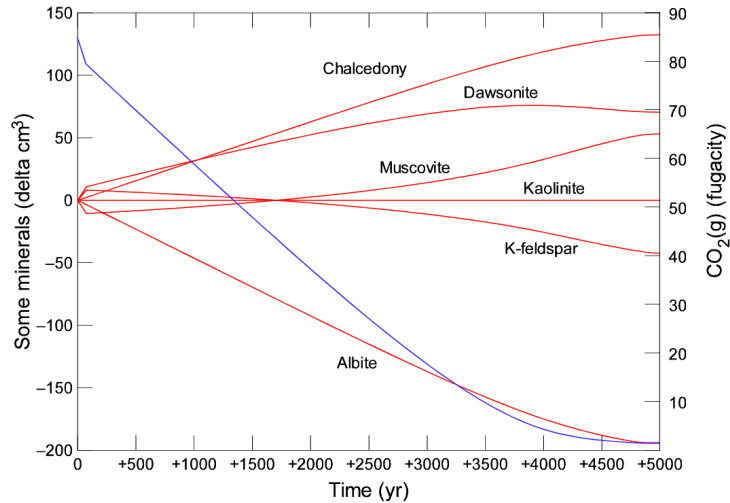
583  
584 As expected, storage of CO<sub>2</sub> in minerals is considerably different between equilibrium and  
585 kinetic models. Figure 6 shows the amount of CO<sub>2</sub> stored by mineral reactions per Kg of water,  
586 in each flow unit. Equilibrium models show storage ranging from 0.4 to 2.7 mol CO<sub>2</sub> per Kg of  
587 water. Kinetic models all show storage of less than 0.2 mol CO<sub>2</sub> per Kg of water, and as low as  
588 0.01 mol CO<sub>2</sub> per Kg of water. The equilibrium models show a strong dependence of CO<sub>2</sub>  
589 storage on flow unit mineralogy. For kinetic models, mineralogical differences have a much  
590 lesser, but still detectable effect over the 50-year injection period. Differences in CO<sub>2</sub> storage  
591 due to mineral reactions for either equilibrium or kinetic simulations primarily reflect dissolution  
592 of greater amounts of muscovite and albite to form dawsonite. Generally, the presence of high  
593 TDS formation water results in formation of more dawsonite, due to the higher Na<sup>+</sup> content of  
594 the saline water, and the resulting storage of more CO<sub>2</sub>. More CO<sub>2</sub> is stored in the low TDS  
595 formation water due to greater solubility. Overall, it is clear that the mineral storage amounts  
596 (22.25 MT) published by Wilson and Monea (2004) based on equilibrium modeling greatly  
597 overestimate mineral storage at Weyburn.

598



599  
 600 Figure 6. Mineral storage of CO<sub>2</sub> by flow unit for equilibrium and kinetic models. “Eum” refers to  
 601 equilibrium models, “Kin” refers to kinetic models “Hi” is high, and “Lo” is low.

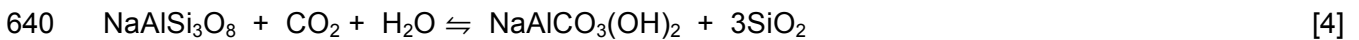
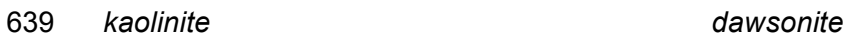
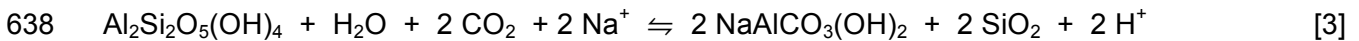
602  
 603 Once injection stops, no more CO<sub>2</sub> is added. The silicates have not come to equilibrium at the  
 604 end of injection (50 years), and will continue to react with the CO<sub>2</sub> remaining in the supercritical  
 605 CO<sub>2</sub> fluid, the saline formation water and the oil. During this stage of modeling, pure supercritical  
 606 CO<sub>2</sub> is no longer being added and the CO<sub>2</sub> present will eventually be consumed by reaction with  
 607 saline water and minerals. Although reaction that continues after injection stops will not change  
 608 the amount of CO<sub>2</sub> that can be stored, it will redistribute the CO<sub>2</sub> in the system. At the end of  
 609 injection CO<sub>2</sub> is present as a supercritical phase and dissolved in oil and saline water. As the  
 610 reservoir “soaks” when injection stops, an increasing amount of CO<sub>2</sub> is trapped in minerals.  
 611 Accordingly, one simulation (Figure 8, M0, high TDS) was completed for 5000 years, with the  
 612 fugacity of CO<sub>2</sub>, the saline water composition, and the amounts of reactive minerals initially set  
 613 to the values at the end of the 50-year injection period. Assuming the pressure and temperature  
 614 at the end of injection are similar to the start of injection, the fCO<sub>2</sub> at 170 bars and 60°C,  
 615 calculated from Duan and Sun (2003) is 85 bars. At the start of the 5000-year simulation, per Kg  
 616 of fluid, there is 116 cm<sup>3</sup> of anhydrite, 2285 cm<sup>3</sup> of calcite, 30 cm<sup>3</sup> of dawsonite, and 5831 cm<sup>3</sup> of  
 617 dolomite. After 5000 years, there is 107 cm<sup>3</sup> of anhydrite, 2302 cm<sup>3</sup> of calcite, 87 cm<sup>3</sup> of  
 618 dawsonite, and 5832 cm<sup>3</sup> of dolomite. Total mineral volume per Kg of water has increased from  
 619 8262 to 8324 cm<sup>3</sup>. As Figure 7 shows, over the 5000 years, the fugacity of CO<sub>2</sub> has decreased  
 620 from 85 bar to 1 bar. Total carbon in the fluid initially is 1.47 mol/Kg and at the end it is 0.04  
 621 mol/Kg, the difference being transferred from the saline formation water, supercritical fluid and  
 622 oil, to the minerals.



623  
 624 Figure 7. Kinetic simulation of M0 flow unit for high TDS saline formation water at 60°C and  
 625 starting  $f\text{CO}_2 = 85$  bar, showing the evolution of mineral amounts at the end of injection over  
 626 5000 years. Red lines represent the difference in mineral amounts. The blue line is the change  
 627 in  $\text{CO}_2$  fugacity. Note that time 0 is after 50 years of  $\text{CO}_2$  injection and no additional  $\text{CO}_2$  is  
 628 added during the simulation.

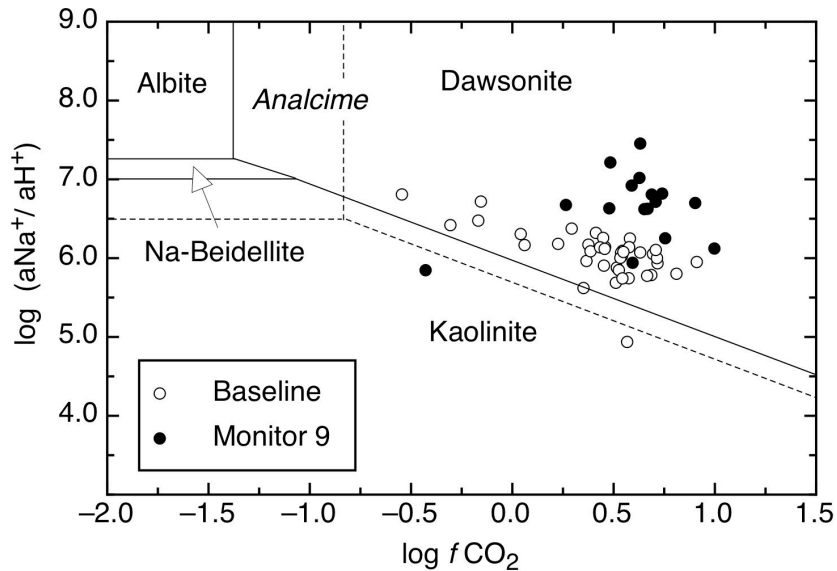
629  
 630 5.2 Dawsonite Formation

631 Analyses of formation waters from the Weyburn reservoir can be compared to the stability of  
 632 dawsonite, relative to kaolinite, albite and Na-beidellite, a component in smectite. Hellevang et  
 633 al. (2005, 2010, 2011 and 2013) suggest that there are significant barriers to dawsonite  
 634 formation. It is not possible to prove with the existing data that dawsonite has formed at  
 635 Weyburn as a result of  $\text{CO}_2$  injection, but produced water and gas analyses are available to  
 636 examine the state of produced waters relative to dawsonite stability. The relevant reactions are:

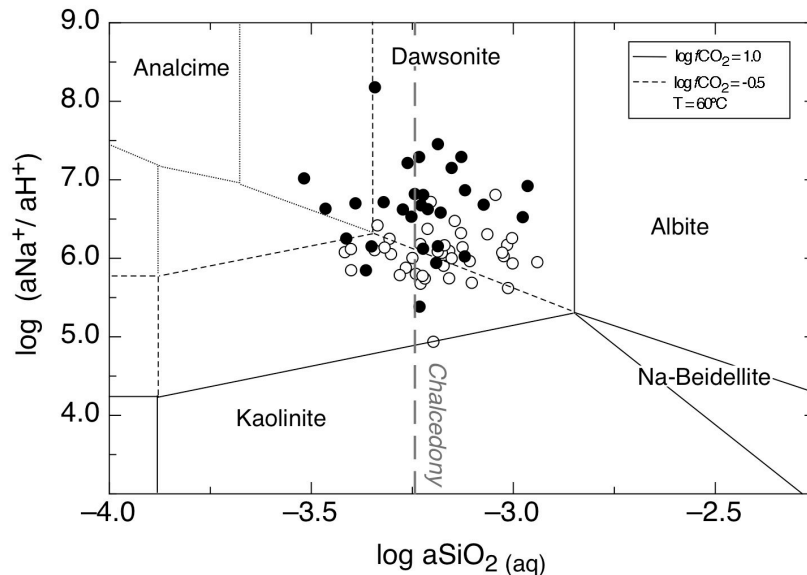


642  
 643 In addition to temperature and pressure, the relevant variables are the fugacity of  $\text{CO}_2$  ( $f\text{CO}_2$ ),  
 644 the activity ratio of  $\text{Na}^+/\text{H}^+$ , and the activity of aqueous  $\text{SiO}_2$ . Two equilibrium phase diagrams,  
 645 similar to those presented by Hellevang et al. (2011) calculated using ACT2 (Geochemists Work

646 Bench®) portray the stability of dawsonite relative to kaolinite, albite and Na-beidellite.  
 647 Hellevang et al. (2013) suggest that analcime may form from albite dissolution rather than  
 648 dawsonite. Figure 8a shows  $\log f\text{CO}_2$  versus the log of the activity ratio of  $\text{Na}^+/\text{H}^+$ , Figure 8b  
 649 shows a  $\text{SiO}_2(\text{aq})$  versus the log of the activity ratio of  $\text{Na}^+/\text{H}^+$ .  
 650



651  
 652



653  
 654 Figure 8. The stability of dawsonite at 60°C and 1 bar. (a) The activity of aqueous  $\text{SiO}_2$  is set by  
 655 equilibrium with chalcedony. Solid boundaries represent stability of dawsonite relative to albite.  
 656 Dashed boundaries represent stability relative to analcime. (b) Dotted lines show analcime  
 657 stability with dawsonite suppressed. Dashed ( $\log f\text{CO}_2 = -0.5$ ) boundaries and solid boundaries

658 (log  $f\text{CO}_2 = 1.0$ ) show the stability of dawsonite relative to albite, kaolinite and Na-beidellite  
659 (smectite). The range of log  $f\text{CO}_2$  at Weyburn is between -0.5 and 1.0.

660

661 Plotted on the phase diagrams (Figure 8a, b) are baseline formation water compositions (open  
662 circles) and produced water compositions from Monitor 9 (M9, 3 years after start of injection,  
663 closed circles). Baseline fluid compositions are from Emberley et al. (2005), M9 fluid  
664 compositions are shown in Table 2. The activity of the requisite species was calculated using  
665 SOLMIN88 (Kharaka et al., 1988) by the methods outlined in Shevalier et al. (2013) to  
666 determine the pH and species activity at reservoir conditions. Figure 8b shows that the water  
667 compositions tend to cluster around saturation with respect to chalcedony. Fluid compositions  
668 from Baseline to M9 trend towards increasing stability of dawsonite, primarily due to decrease in  
669 pH between baseline and M9 (Shevalier et al., 2013). Mineral species that exist as solid  
670 solutions will have lower activities of the thermodynamic component (e.g., the Na-feldspar albite  
671 as a component in plagioclase), and this will cause the stability fields to enlarge. However, at  
672 Weyburn the plagioclase is observed to be primarily albite component, and the other minerals  
673 (kaolinite, analcime and dawsonite) show little or no solid substitution, therefore the stability  
674 fields are unaffected. An exception is Na-beidellite, a component of smectite. If smectite were to  
675 form during  $\text{CO}_2$  injection, the activity of Na-beidellite (the Na component in the mineral  
676 smectite) would likely be less than one, and this could cause a significant increase in the  
677 stability field, potentially causing Na-beidellite to encompass the observed fluid composition  
678 range to the exclusion of dawsonite and analcime. No post- $\text{CO}_2$  core was available from  
679 Weyburn, so the possible existence of dawsonite or smectite (beidellite) as a product of  $\text{CO}_2$   
680 injection is not known. Modeling by Abercrombie et al. (1994) suggests that silica activities, that  
681 range from -3.5 to -3.0 by Monitor 9 (Figure 8), are within the range necessary to precipitate  
682 smectite. Our modeling also shows that other zeolite minerals, including mordenite and  
683 clinoptilolite, are more stable than dawsonite and need to be suppressed to present the stability  
684 field of dawsonite. It is not known if any zeolite minerals have formed as a result of  $\text{CO}_2$  injection  
685 at Weyburn, so the relative stability of these zeolites was not pursued.

686

687 The composition of produced fluids suggests that water compositions resulting from injection of  
688  $\text{CO}_2$  are within the stability field of dawsonite and that injection of  $\text{CO}_2$  favours increased  
689 stability of dawsonite. Figure 5 shows a kinetic reaction path simulation showing dawsonite may  
690 begin to precipitate as muscovite (source of aluminum) dissolves and this may occur within 5-10  
691 years of commencement of  $\text{CO}_2$  injection. However, these observations do not require that

692 dawsonite actually forms or persists. Nucleation difficulties and the availability of sufficient  $\text{Al}^{3+}$   
693 in solution could prevent or attenuate dawsonite precipitation (Hellevang et al., 2013). Further,  
694 at Weyburn the dissolution of potential silicate precursors (albite, kaolinite and K-feldspar) is  
695 probably overestimated as they occur in small amounts (0.3-9 wt%) and are not totally exposed  
696 to the injected fluids. Further, the dissolution of silicate precursors and the precipitation of  
697 dawsonite could be inhibited by the presence of oil in the porosity. In the absence of  
698 examination of post-injection core it is not possible to determine whether or not dawsonite has  
699 formed in the Weyburn reservoir.

700

#### 701 **6. Storage of $\text{CO}_2$ in Minerals, Gas, Oil and Saline water**

702 To estimate potential storage of  $\text{CO}_2$  at Weyburn requires estimates of the pre-injection amount  
703 of  $\text{CO}_2$  in each phase (oil, gas, saline water, minerals) and the final amounts in those phases.  
704 Geochemical simulations, combined with the pore volume saturated with saline water, allow an  
705 estimate of  $\text{CO}_2$  stored in saline formation water and minerals during 50 years of injection at  
706 Weyburn. White et al. (2004) give starting oil saturation as 0.53 in the Marly and 0.35 in the  
707 Vuggy. Because only saline formation water and oil (at the start of injection there is no free gas  
708 phase present) are present prior to  $\text{CO}_2$  injection, saline water saturations are 0.47 in the Marly  
709 and 0.65 in the Vuggy. However, at the end of injection,  $\text{CO}_2$  also will be resident in  
710 unrecoverable oil (irreducible oil) and in a remaining supercritical  $\text{CO}_2$ -rich fluid phase. The  
711 additional information required to estimate  $\text{CO}_2$  storage in the Phase 1A area at Weyburn  
712 includes:

- 713 1. The total pore volume of each flow unit.
- 714 2. The starting and ending saturation of that pore volume with oil, saline water and  $\text{CO}_2$   
715 supercritical fluid.
- 716 3. The initial and final amount of  $\text{CO}_2$  in oil.
- 717 4. The starting and ending amount and composition of the  $\text{CO}_2$  supercritical fluid phase.

718

719 Table 4 shows the pore volume of major units at Weyburn (Geoff Burrowes and Stan Wright,  
720 Cenovus, personal communication). In the Phase 1A area the Marly has a pore volume of  
721 approximately  $34 \cdot 10^6 \text{ m}^3$  and the Vuggy has a pore volume of approximately  $40 \cdot 10^6 \text{ m}^3$ . Within  
722 the Marly the greatest pore volume is in the M3 flow unit ( $16.8 \cdot 10^6 \text{ m}^3$ ) and in the Vuggy the  
723 greatest pore volume is in the V2 ( $15.4 \cdot 10^6 \text{ m}^3$ ) flow unit. The relative volume fraction  
724 saturations at the end of  $\text{CO}_2$  injection with respect to oil-water-gas for the Marly are projected

725 to be 0.3/0.5/0.2 and 0.2/0.7/0.1 for the Vuggy (Geoff Burrowes and Stan Wright, Cenovus,  
726 personal communication).

727



**Table 4. Pore Volume (m<sup>3</sup>) of Flow Units, Weyburn Phase 1A Area.**

<b>Flow Unit</b>	<b>Volume (m<sup>3</sup>)</b>
Marly (All flow units)	3.40E+07
Vuggy (All flow units)	3.99E+07
Marly M0	5.31E+06
Marly M1	9.54E+06
Marly M2	2.37E+06
Marly M3	1.68E+07
Vuggy V1	6.90E+06
Vuggy V2	1.54E+07
Vuggy V3	1.99E+06
Vuggy V4	4.27E+06
Vuggy V5	4.61E+06
Vuggy V6	6.72E+06

728

729 The amount of CO<sub>2</sub> stored as minerals and saline formation water is estimated from the reaction  
730 path simulations. For the estimates presented below, only the kinetic results are used. It is

731 assumed that at the end of injection, the supercritical fluid is 100% CO<sub>2</sub>. From the fluid-  
732 saturated pore volume, the molar amount of CO<sub>2</sub> stored in supercritical fluid CO<sub>2</sub> can be  
733 calculated from the specific volume of CO<sub>2</sub> (65.75 cm<sup>3</sup>/mol at 60°C and 170 bar: Duan et al,  
734 1992).

735

736 The way in which injected supercritical CO<sub>2</sub> behaves with respect to the reservoir geometry, and  
737 dissolution in oil and saline formation water is complex. Detailed reservoir modeling, not  
738 attempted here, is required to determine distribution of CO<sub>2</sub> (and other gas species) during the  
739 injection period. To obtain an estimate of the amount of CO<sub>2</sub> in saline water, oil and as a gas or  
740 supercritical phase, we consider only the initial (pre injection) and final (end of injection) state.  
741 The injection of supercritical CO<sub>2</sub> may bypass the oil zones due to buoyancy override and arrive  
742 directly at production wells. During Weyburn oil field operations, CO<sub>2</sub> at producing wells is  
743 captured and re-cycled into injection wells. A zone of supercritical CO<sub>2</sub> may be present within  
744 the upper part of the reservoir units at Weyburn, but the extent of such a phase, if present, is  
745 unknown. However, a significant fraction of the injected supercritical CO<sub>2</sub> dissolves in the oil, as  
746 evidenced by the data of You et al. (2013). At Weyburn in the Phase 1A area there was no free  
747 gas phase present before CO<sub>2</sub> injection, therefore no CO<sub>2</sub> (or any other species) is present as  
748 gas initially at the reservoir level. However, prior to CO<sub>2</sub> injection, pressure drop during  
749 production causes CO<sub>2</sub>, H<sub>2</sub>S, CH<sub>4</sub> and higher carbon number (at least up to C<sub>5</sub>) gas species that  
750 initially are dissolved in oil and saline water, to be produced at surface. After injection started in  
751 September of 2000, the fraction of CO<sub>2</sub> produced as a gas at surface, increased with time  
752 (Mayer et al., 2013). Continued injection of CO<sub>2</sub> is expected to eventually produce either a gas  
753 or supercritical CO<sub>2</sub>-rich fluid phase at the reservoir level and once this has formed, it is  
754 expected that the CO<sub>2</sub>, H<sub>2</sub>S, CH<sub>4</sub> and higher carbon number gas species will be distributed  
755 between the saline formation water, oil and a gas/supercritical fluid phase.

756

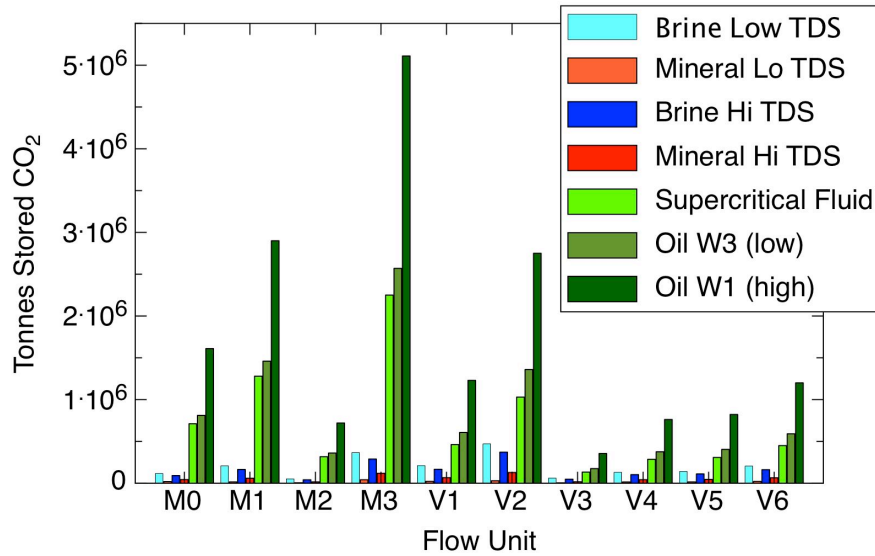
757 The calculation for CO<sub>2</sub> solubility in oil assumes that CO<sub>2</sub> comes rapidly (within years) to  
758 solubility equilibrium with the oil. Only the starting (pre CO<sub>2</sub> injection) and final (end of CO<sub>2</sub>  
759 injection) amounts are considered, thus the amount of CO<sub>2</sub> in oil will be maximized. Pre injection  
760 concentrations of CO<sub>2</sub> in oil are less than 5 mol % (Srivastava et al., 2000). Results from You et  
761 al. (2013) show that after ten years, CO<sub>2</sub> content of the oils is as high as 38.5 mol percent,  
762 confirming that CO<sub>2</sub> is dissolving rapidly in the oil. The initial amount of CO<sub>2</sub> in oil is calculated  
763 from the results of Srivastava et al. (2000) and the pore volume fraction saturated with oil. The  
764 ending amount is calculated from the final oil saturated pore volume and the solubility of CO<sub>2</sub> in

765 oil as calculated according to procedures described in the Methods section. The difference  
766 between the initial CO<sub>2</sub> in oil and the final amount of CO<sub>2</sub> in oil at elevated pCO<sub>2</sub> represents  
767 additional CO<sub>2</sub> storage in oil. As previously noted, the greater buoyancy of a CO<sub>2</sub> rich  
768 supercritical phase might cause it to bypass some of the oil within the reservoir, reducing the  
769 total amount of CO<sub>2</sub> estimated to be captured in oil at Weyburn. Detailed reservoir modeling,  
770 incorporating flow and the distribution of gas, comprised of CO<sub>2</sub>, H<sub>2</sub>S and C<sub>1</sub>-C<sub>5+</sub> hydrocarbons,  
771 is required to estimate the degree of this effect. Such modeling is beyond the scope of this  
772 paper.

773

774 Combining the results of mineral, saline formation water, gas and oil calculations and the pore  
775 volume saturated with saline water, gas and oil at the end of injection, allows the total storage of  
776 CO<sub>2</sub> to be calculated for Phase 1A at Weyburn at the end of injection (here assumed to be 50  
777 years). Figure 9 shows, by flow unit, the total tonnes of CO<sub>2</sub> in saline formation water (low and  
778 high TDS), minerals (low and high TDS), oil (W1 and W3, representing high and low solubility,  
779 respectively) and gas or supercritical fluid. The following numbers need to be placed in the  
780 context that between 2000 and 2012, 22 million tonnes of CO<sub>2</sub> have been injected over the  
781 entire Weyburn field (Petroleum Technology Research Centre, 2014), although this number is  
782 certainly greater at the time of writing and will increase until the end of the oil recovery project.  
783 Total storage of CO<sub>2</sub> in Phase 1A dissolved in oil is the largest sink, ranging from 6.5•10<sup>6</sup> to  
784 1.3•10<sup>7</sup> tonnes, depending on solubility. Storage in the supercritical CO<sub>2</sub>-rich phase, is  
785 significant, approximately 7.2•10<sup>6</sup> tonnes, and greater than in minerals (range from 2-6•10<sup>5</sup>  
786 tonnes) and saline formation water (range from 1.5-2•10<sup>6</sup> tonnes). Storage of CO<sub>2</sub> by solubility  
787 in the oil, even after the reservoir has been depleted near to irreducible oil saturation, is greater  
788 than storage in the supercritical CO<sub>2</sub> phase, in saline water and in minerals.

789



790  
791

792 Figure 9. Storage of CO<sub>2</sub> in supercritical fluid, saline formation water, minerals and oil at the end  
793 of 50 years of injection at the Phase 1A area in Weyburn.

794

## 795 7. Discussion

796

797 By the calculations outlined above, oil at Weyburn Phase 1A represents potentially the largest  
798 sink for injected CO<sub>2</sub>, even though oil represents by volume only 30% and 20% respectively, of  
799 the estimated final pore saturation of the Marly and Vuggy flow units. This is primarily due to the  
800 fact that at Weyburn the oil is high API gravity (low density), has relatively high CO<sub>2</sub> solubility  
801 and, prior to CO<sub>2</sub> injection, has a very low amount of dissolved CO<sub>2</sub>. Also, prior to injection of  
802 CO<sub>2</sub> the oil has very low gas saturation, and there is no free gas phase in the reservoir. Further,  
803 the gas components initially dissolved in oil include H<sub>2</sub>S and C<sub>1</sub>-C<sub>5+</sub> hydrocarbon gas, in addition  
804 to relatively low amounts of CO<sub>2</sub> (Emberley et al., 2005), therefore CO<sub>2</sub> initially represents a  
805 relatively small proportion of the gas species dissolved in oil. The very high CO<sub>2</sub> solubility of  
806 Weyburn oil, combined with the low amount of CO<sub>2</sub> in oil and saline water prior to CO<sub>2</sub> injection,  
807 results in significant calculated storage of CO<sub>2</sub> in oil at the end of injection. In addition, relatively  
808 short-term (50+ years) storage in oil at Weyburn is comparatively secure. At the end of injection  
809 of CO<sub>2</sub> and economic oil recovery, most of the oil is trapped in the pore volume by strong  
810 capillary forces. Only a catastrophic decrease in pressure would release the CO<sub>2</sub> from solution  
811 in the oil.

812

813 Various factors will affect the calculated versus the actual amounts of CO<sub>2</sub> stored at Weyburn  
814 over the 50-year injection period. The amount of solubility storage in oil is strongly dependent on  
815 the final oil saturations, which are unknown and will be variable across the Weyburn field.  
816 Further, the solubility data for CO<sub>2</sub> in oil are restricted to the northern part of the Weyburn field.  
817 Generally oil density (Figure 1) decreases (API gravity increases) over the rest of the Weyburn  
818 field, so storage in oil will probably be at least equal to the highest measured value, 640 sm<sup>3</sup>/m<sup>3</sup>,  
819 or greater. Finally, as noted previously, buoyancy override of supercritical CO<sub>2</sub> may cause oil  
820 saturated zones to be bypassed, causing the amount of CO<sub>2</sub> captured in oil to be less than  
821 calculated here. Regardless of the unknown effect of the variation of CO<sub>2</sub> solubility in Weyburn  
822 oil, and bypassing of oil zones, solution of CO<sub>2</sub> in oil will probably be the dominant form of  
823 storage at Weyburn at the end of CO<sub>2</sub> injection.

824  
825 The mineral surface areas and reaction rates in our calculations are poorly known. In our  
826 calculations, precipitation rates are assumed to be the same as dissolution rates, but are  
827 probably slower. Effective mineral surface areas are probably smaller than those used in  
828 simulations, further reducing the rate of reaction. Further, the presence of oil possibly wetting  
829 mineral surfaces (Yang et al., 2008) will decrease surface areas even more, resulting in less  
830 mineral storage of injected CO<sub>2</sub>. Thus, the mineral estimates for the injection period (50 years)  
831 probably represent maximum mineral storage. Further, redistribution of injected CO<sub>2</sub> from the  
832 oil, saline formation water, and supercritical fluid to the minerals requires approximately 5000  
833 years in the calculations presented, but because the mineral reaction rates are probably slower  
834 than those used here, this probably is a minimum time estimate.

835  
836 The calculations do not couple flow, reaction rates and the resulting storage. Such calculations  
837 were not attempted. Although reactive transport is an important consideration, the data  
838 gathering required to frame these calculations leaves this as a next step to refine the results  
839 presented here. An outline of proposed reactive transport modeling at Weyburn is given in  
840 Johnson et al. (2011). Cavanagh and Rostron (2013) used high-resolution capillary flow  
841 simulations of migration pathways and recognize that the large number of wells and high well  
842 density in the Weyburn field result in a major challenge for conventional flow modelling.

843  
844 The results presented here are for the Phase 1A area of the IEA GHG Weyburn Monitoring and  
845 Storage Project. However, they can be extrapolated to the entire Weyburn field if we assume  
846 that the mineralogy of the various flow units is similar to that determined for the Phase 1A area.

847 The resulting potential storage for the entire field would increase to approximately  $1.7 \cdot 10^8$   
848 tonnes of injected  $\text{CO}_2$  from  $2.3 \cdot 10^7$  for only the Phase 1A area.

849

850

## 851 **8. Conclusions**

852 1. Over a 50-year injection period at Weyburn Phase 1A,  $\text{CO}_2$  dissolved in oil is the  
853 dominant form of  $\text{CO}_2$  storage ( $6.5 \cdot 10^6$  to  $1.3 \cdot 10^7$  tonnes), followed closely by  
854 storage as a supercritical  $\text{CO}_2$  phase ( $7.2 \cdot 10^6$  tonnes). Storage of injected  $\text{CO}_2$  in  
855 saline formation water (range from  $1.5 \cdot 10^6$  to  $2 \cdot 10^6$  tonnes) and mineral storage (range  
856 from  $2 \cdot 10^5$  to  $6 \cdot 10^5$  tonnes) are the smallest sinks. No additional  $\text{CO}_2$  will be stored other  
857 than that injected over the 50 year period.

858 2. Simulations show that  $\text{CO}_2$  present as a supercritical fluid, saline water, and  
859 dissolved in oil at the end of injection is redistributed over a period of at least 5000  
860 years into dawsonite. However, it is not possible to show conclusively that dawsonite  
861 has formed at Weyburn. Other Na-silicates including zeolites, and clay minerals may  
862 form, but were not included in estimates of  $\text{CO}_2$  mineral storage.

863 3. Although the Vuggy and Marly flow units have variable mineralogy, the modeled  
864 reactions that take place due to addition of  $\text{CO}_2$  are similar. Simulations that consider  
865 the mineralogy of individual flow units, and thereby the effect of variations in  
866 mineralogy on storage of  $\text{CO}_2$  in oil, saline formation water, and minerals, represent  
867 a second order influence on  $\text{CO}_2$  storage at Weyburn.

868 4. The availability of Na, either dissolved in saline water or available in minerals such  
869 as plagioclase (albite), is an important factor in long-term mineral storage of  $\text{CO}_2$ ,  
870 due to the probable formation of dawsonite. Increased TDS, and thereby the amount  
871 of Na available in saline water, will increase the amount of  $\text{CO}_2$  potentially stored in  
872 Na-containing minerals. It is also expected that the amount of  $\text{CO}_2$  stored in saline  
873 formation water will decrease as TDS increases, due to the decrease in solubility of  
874  $\text{CO}_2$  with increasing TDS.

875 5. Projects targeting abandoned oil reservoirs as possible storage sites for  $\text{CO}_2$  should  
876 focus on sites that have no gas phase at reservoir level and an oil phase that has  
877 initially low  $\text{CO}_2$  content, but very high  $\text{CO}_2$  solubility. Typically, these conditions will  
878 be present in relatively shallow reservoirs with oils of high API gravity (low density).  
879 The capillary trapping forces at the end of oil recovery will result in oil being a  
880 relatively secure storage sink for injected  $\text{CO}_2$  over the short term of 100's of years.

881 Over the longer term of thousands to tens of thousands of years, the CO<sub>2</sub> dissolved  
882 in saline formation water, supercritical fluid, and oil will be redistributed into mineral  
883 phases, if sufficient volumes of reactive minerals are present.

## References

- Abercrombie, H.J., Hutcheon, I.E., Bloch, J.D. and de Caritat, P., 1994. Silica activity and the smectite-illite reaction. *Geology* 22, 539-542.
- Assayag, N., Matter, J., Ader, M., Goldberg, D and Agriner, P., 2009. Water–rock interactions during a CO<sub>2</sub> injection field test: Implications on host rock dissolution and alteration effects. *Chemical Geology* 265, 227-235.
- Baker, J.C., 1991. Diagenesis and reservoir quality of the Aldebaran Sandstone, Denison Trough, eastcentral Queensland, Australia. *Sedimentology* 38, 819-838.
- Baker, J.C., Guo, P.B., Hamilton, P.J., Golding, S.D., Keene, J.B., 1995. Continental-scale magmatic carbon dioxide seepage recorded by Dawsonite in the Bowen-Gunnedah-Sydney basin system, Eastern Australia. *Journal of Sedimentary Research* A65, 522-530.
- Burrowes, G., 2001. Investigating CO<sub>2</sub> Storage Potential of Carbonate Rocks during Tertiary Recovery from a Billion Barrel Oil field, Weyburn, Saskatchewan: Part 2 - Reservoir Geology (IEA Weyburn Monitoring and Storage Project) Saskatchewan Energy Mines Miscellaneous Report 2001-4, 64-72.
- Burrowes, G., Gilboy, C. 2000., Investigating Sequestration Potential of Carbonate Rocks During Tertiary Recovery from a Billion Barrel Oil Field, Weyburn, Saskatchewan: The Geoscience Framework. IEA Weyburn CO<sub>2</sub> Monitoring and Storage Project Report., 2000.
- Cantucci, B., Montegrossi, G., Vaselli, O., Tassi, F., Quattrocchi, F., Perkins, E., 2009. Geochemical modeling of CO<sub>2</sub> storage in deep reservoirs: The Weyburn Project (Canada) case study. *Chemical Geology* 265, 181-197.
- Cavanagh, A. and Rostron, B., 2013. High-resolution simulations of migration pathways and the related potential well risk at the IEAGHG Weyburn–Midale CO<sub>2</sub> storage project. *International Journal of Greenhouse Gas Control* 16S, S15-S24.
- de Caritat, P., Bloch, J., and Hutcheon, I., 1994. LPNORM: a linear programming normative analysis code. *Computers and Geoscience* 20, 313-347.
- Duan, Z., Sun, R., 2003. An improved model calculating CO<sub>2</sub> solubility in pure water and aqueous NaCl solutions from 273 to 533 K and from 0 to 2000 bar. *Chemical Geology* 193, 257-271.
- Duan, Z.H., Moller, N., and Weare, J.H., 1992. An equation of state (EOS) for CH<sub>4</sub>-CO<sub>2</sub>-H<sub>2</sub>O I: pure systems from 0 to 1000 C and from 0 to 8000 bar. *Geochimica et Cosmochimica Acta* 56, 2605-2617.
- Dunham, R.J., 1962. Classification of carbonate rocks according to depositional textures. In *Classification of Carbonate Rocks*, edited by W.E. Ham, 08-121. American Association of Petroleum Geologists Memoir 1.
- Durocher, K., Hutcheon, I., Shevalier, M., Mayer, B., Gunter, B., Perkins, E., Bloch, J., 2003. *Subtask 3.1: Reservoir (Baseline) Mineralogy Final Report*. IEA Weyburn CO<sub>2</sub> Monitoring and Storage Project, Regina: Petroleum Technology Research Centre.
- Durocher, K.E., Bloch, J., Perkins, E., Hutcheon, I., Shevalier, M., Mayer, B. and Gunter, W.D., 2005. Mineralogical Characterization of the Weyburn Reservoir, Saskatchewan, Canada: are mineral reactions driving injected CO<sub>2</sub> storage? Edited by M., Morris, T., Gale, J. and Thambimuthu, K. Wilson. *Proceedings of the 7th International Conference on Greenhouse Gas Control Technologies*. Oxford: Elsevier 2097-2101.
- Emberley, S., Hutcheon, I., Shevalier, M., Durocher, K., Mayer, B., Günter, W.D., Perkins, E.H., 2005. Monitoring of fluid-rock interaction and CO<sub>2</sub> storage through produced fluid



- sampling at the Weyburn CO<sub>2</sub>-injection enhanced oil recovery site, Saskatchewan, Canada. *Applied Geochemistry* 20, 1131-1157.
- Ferrini, V., Martarelli, L., De Vito, C., Cina, A and Deda, T., 2003. The Koman dawsonite and realgar-orpiment deposit, northern Albania; inferences on processes of formation. *The Canadian Mineralogist* 41, 413-427.
- Gunter, W.G., Perkins, E.H., Hutcheon, I., 2000. Aquifer disposal of acid gases: modeling of water-rock reactions for trapping of acid waters. *Applied Geochemistry* 15, 1086-1096.
- Gunter, W.G., Bachu, S., Benson, S., 2004. The role of hydrogeological and geochemical trapping in sedimentary basins for secure geological storage of carbon dioxide. *Geological Society of London, Special Publication* 233, 129-145.
- Hellevang, H., Aagaard, P., Oelekers, P., Kvamme, B., 2005. Can dawsonite permanently trap CO<sub>2</sub>? *Environmental Science and Technology* 39, 8281-8287.
- Hellevang H, Declercq J, Kvamme B and Aagaard P., 2010. The dissolution rate of dawsonite at pH 0.9 to 5 and temperatures of 22, 60 and 77 °C. *Applied Geochemistry* 25, 1575-1586.
- Hellevang, H., Declercq, J., Aagaard, P., 2011. Why is Dawsonite Absent in CO<sub>2</sub> Charged Reservoirs? *Oil & Gas Science and Technology* 66, 119-135.
- Hellevang, H., Aagaard, P., and Jahren, J., 2013. Will dawsonite form during CO<sub>2</sub> storage? *Greenhouse Gas Science and Technology* 4, 191-199.
- Hitchon, B., 2012. *Best Practices for Validating CO<sub>2</sub> Geological Storage: Observations and Guidance From the IEAGHG Weyburn Midale CO<sub>2</sub> Monitoring and Storage Project*. Edited by Brian Hitchon. Sherwood Park, Alberta: Geoscience Publishing. 353 p.
- Holm, L.W. and Josendal, V.A., 1974. Mechanism of oil displacement by carbon dioxide. *Journal of Petroleum Technology (Transaction AIME)* 257, 1427-1438.
- Holm, L.W., 1959. Carbon dioxide solvent flooding for increased oil recovery processes. *Petroleum Transactions* 216, 225-231.
- Hovorka, S., Benson, S., Doughty, C., Freifeld, B.M., Sakurai, S., Daley, T., Kharaka, Y., Holtz, M., Trautz, R.C., Seay Nance, H., Myer, L.R., and Knauss, K.G., 2006. Measuring permanence of CO<sub>2</sub> storage in saline formations: the Frio experiment. *Environmental Geosciences* 13, 105-121.
- Hutcheon, I., Shevalier, M., and Abercrombie, H.J., 1993. pH buffering by metastable mineral-fluid equilibria and evolution of carbon dioxide fugacity during burial diagenesis. *Geochimica et Cosmochimica Acta* 57, 1017-1027.
- IPCC (Intergovernmental Panel on Climate Change). *Prepared by Working Group III of the Intergovernmental Panel on Climate Change*. Edited by B., Davidson, O., de Coninck, H.C., Loos, M., Mayer, L.A. (Eds.) In: Metz. Cambridge, United Kingdom/New York, NY, USA.: Cambridge University Press, 2005.
- Jensen, G.K.S., Nickel, E.H., and Rostron, B.J., 2013. Refinement of the Weyburn-Midale geological and hydrogeological model: Developing a better framework to determine reservoir response to injected CO<sub>2</sub> and subsequent CO<sub>2</sub> movement. *International Journal of Greenhouse Gas Control* 16S, S5-S14.
- Johnson, J.W., Mayer, B., Shevalier, M., Perkins, E., Talman, S., Kotzer, T., Hawkes, C., Butler, S., Luo, M., Er, V., Ramirez, A., Carroll, S., Wolery, T., McNab, W., Hao, Y., Carle, S., Jones, D., Beaubien, S., and Le Pierres, K., 2011. Geochemical assessment of isolation performance during 10 years of CO<sub>2</sub> EOR at Weyburn. *Energy Procedia* 4, 3658-3665.
- Kharaka, Y. K., Gunter, W., Aggarwal, P. K., Perkins, E. H. and De Braal, J. D., 1988. SOLMINEQ88: a computer programme for geochemical modelling of water-rock reactions. *USGS Water Resources Investigation Report* 88-4227.

- Kharaka, Y., Cole, D.R., Hovorka, S.D., Gunter, W.D., Knauss, K.G., Freifeld, B.M., 2006 Gas-water-rock interactions in Frio Formation following CO<sub>2</sub> injection: Implications for the storage of greenhouse gases in sedimentary basins. *Geology* 34, 577-580.
- Lasaga, A.C., 1984. Chemical kinetics of water-rock interactions. *Journal of Geophysical Research*. 89, 4009-4025.
- Matter, J M., Martin S., Snæbjörnsdóttir, S. Ó., Oelkers, E.H., Gislason S. R., Aradóttir, E. S., Sigfusson, B., Gunnarsson, I., Sigurdardóttir, H., Gunnlaugsson, E., Axelsson, G., Alfredsson, H.A., Wolff-Boenisch, D., Mesfin, K., D. Fernandez de la Reguera Taya, Hall, J., Dideriksen, K., and Broecker, W.S. 2016. Rapid carbon mineralization for permanent disposal of anthropogenic carbon dioxide emissions. *Science* 10, 1312-1314.
- Mayer, B., Shevalier, M., Nightingale, M., Kwon, J-S., Johnson, G., Raistrick, M., Hutcheon, I., and Perkins, E., 2013. Tracing the movement and the fate of injected CO<sub>2</sub> at the IEA GHG Weyburn-Midale CO<sub>2</sub> Monitoring and Storage project (Saskatchewan, Canada) using carbon isotope ratios. *International Journal of Greenhouse Gas Control* 16, S177-S184.
- Mungan, N., 1981. Carbon dioxide flooding fundamentals. *Journal of Canadian Petroleum Technology* 20, 87-92.
- Omotoso, O., McCarty, D.K., Hillier, S., Kleeberg, R., 2006. Some successful approaches to quantitative mineral analysis as revealed by the 3rd Reynolds Cup contest. *Clays and Clay Minerals* 54, 748-760.
- Palandri, J.L., and Kharaka, Y.K., 2004. A Compilation of Rate Parameters of Water-Mineral Interaction Kinetics for Application to Geochemical Modeling. U.S. Geological Survey Open File Report 2004-1068, p. 74.
- Perez, R.J., Shevalier, M., Hutcheon, I., Mayer, B., 2006. A model for partitioning gases among brines and hydrocarbons in oil reservoirs: Examples from the IEA-GHG Weyburn CO<sub>2</sub> Monitoring and Storage Project, Saskatchewan, Canada. *Journal of Geochemical Exploration* 89, 326-330.
- Petroleum Technology Research Centre, 2014. **What Happens When CO<sub>2</sub> is Stored Underground? Q&A from the IEAGHG Weyburn-Midale CO<sub>2</sub> Monitoring and Storage Project. Global Carbon Capture and Storage Institute Limited, Melbourne. 51 pages.**
- Qing, H., Nimegeers, A.R., 2008. Lithofacies and depositional history of Midale carbonate-evaporite cycles in a Mississippian ramp setting, Steelman-Bienfait area, southeastern Saskatchewan, Canada. *Bulletin of Canadian Petroleum Geology* 56, 209-232.
- Raistrick, M., Mayer, B., Shevalier, M., Perez, R., Hutcheon, I., Perkins, E.H., Gunter, W.D., 2006. Using chemical and isotopic data to quantify ionic trapping of carbon dioxide in oilfield brines. *Environmental Science and Technology* 40, 6744-6749.
- Shevalier, M., Nightingale, M., Mayer, B., Hutcheon, I., Durocher, K., Perkins, E., 2013. Brine geochemistry changes induced by CO<sub>2</sub> injection observed over a 10 year period in the Weyburn oil field. *International Journal of Greenhouse Gas Control* 16S, S160-S176.
- Srivastava, R.K., Huang, S.S. and Dong. M., 2000. Laboratory Investigation of Weyburn CO<sub>2</sub> Miscible Flooding. *Journal of Canadian Petroleum Technology* 39, 41-51.
- Srivastava, R.K., Huang, S.S. 1997. Laboratory investigation of Weyburn CO<sub>2</sub> miscible flooding. *7th Saskatchewan Petroleum Conference*. Regina, 1997.
- Steefel, C.I., and Lasaga, A.C., 1994. A coupled model for transport of multiple chemical species and kinetic precipitation/dissolution reactions with application to reactive flow in a single phase hydrothermal system. *American Journal of Science* 294, 529-592.
- Verma, M.K. 2015. Fundamentals of Carbon Dioxide-Enhanced Oil Recovery (CO<sub>2</sub>-EOR)—A Supporting Document of the Assessment Methodology for Hydrocarbon Recovery Using CO<sub>2</sub>-EOR Associated with Carbon Sequestration. Open-File, U.S. Department of the Interior, United States Geological Survey, USGS, 2015, p. 19.

- White, D.J. and Johnson, J.W. 2009. Integrated geophysical and geochemical research programs of the IEA GHG Weyburn-Midale CO<sub>2</sub> monitoring and storage project. *Energy Procedia* 1, 2349-2356.
- White, D.J., Hirsche, K., Davis, T., Hutcheon, I., Adair, R., Burrowes, G., Graham, S., Bencini, R., Majer, E., Maxwell, S.C. 2004., Theme 2: prediction, monitoring, and verification of CO<sub>2</sub> movements." Edited by M., Monea, M. (Eds.), In: Wilson. *IEA GHG Wey-burn CO<sub>2</sub> Monitoring and Storage Project Summary Report 2000–2004*. Regina: Petroleum Technology Research Centre. 73-148.
- Wilson, M., Monea, M., 2004. IEA GHG Weyburn CO<sub>2</sub> Monitoring and Storage Project Summary Report 2000–2004. Petroleum Technology Research Centre, Regina, Canada. p. 273.
- Worden, R.H., 2006. Dawsonite cement in the Triassic Lam Formation, Shabwa Basin, Yemen: A natural analogue for a potential mineral product of subsurface CO<sub>2</sub> storage for greenhouse gas reduction. *Marine and Petroleum Geology*, 23, 61-77.
- Xu., T., Apps, J.A., and Pruess, K., 2004. Numerical simulation of CO<sub>2</sub> disposal by mineral trapping in deep aquifers. *Applied Geochemistry* 19, 917-936.
- Xu, T., Kharaka, Y., Doughty, C., Freifeld, B. and Daley, T.M., 2010. Reactive transport modeling to study changes in water chemistry induced by CO<sub>2</sub> injection at the Frio-I brine pilot. *Chemical Geology* 271, 153-164.
- Yang, D., Gu, Y., Tontiwachwuthikul, P. 2008. Wettability determination of the reservoir brine-reservoir rock system with dissolution of CO<sub>2</sub> at high pressures and elevated temperatures. *Energy and Fuels* 22, 504-509.
- Yuo, P., Vahapcan, E., Freitag, N., Huang, S., 2013. Recharacterizing evolving fluid and PVT properties of Weyburn oil–CO<sub>2</sub> system. *International Journal of Greenhouse Gas Control* 16S, S226-S235.

## FIGURE CAPTIONS

Figure 1. Location map of the Weyburn field in southern Saskatchewan, Canada. The phase 1A area is shown in the shaded area of the inset. The inset map of the Weyburn field is contoured for values of oil API gravity. W1, W2 and W3 are the locations of wells with measured solubility of CO<sub>2</sub> in oil from Srivastava et al. (2000).

Figure 2. Representative petrography and mineral abundance data for the Midale Marly M0 flow unit. Thin section field of view is 500 μm. Scale bar on the SEM photomicrograph is 10 μm.

Figure 3. Representative petrography and mineral abundance data for the Midale Vuggy V2 flow unit. Thin section field of view is 500 μm. Scale bar on the SEM photomicrograph is 100 μm.

Figure 4. Equilibrium reaction path simulation of addition of CO<sub>2</sub> to M0 flow unit at 60°C and 1 bar.

Figure 5. Kinetic reaction path simulation of addition of CO<sub>2</sub> to M0 flow unit at 60°C and 1 bar.

Figure 6. Mineral storage of CO<sub>2</sub> by flow unit for equilibrium and kinetic models. “Eum” refers to equilibrium models, “Kin” refers to kinetic models “Hi” is high, and “Lo” is low.

Figure 7. Kinetic simulation of M0 flow unit for high TDS saline formation water at 60°C and starting  $f\text{CO}_2 = 85$  bar, showing the evolution of mineral amounts at the end of injection over 5000 years. Red lines represent the difference in mineral amounts. The blue line is the change in CO<sub>2</sub> fugacity. Note that time 0 is after 50 years of CO<sub>2</sub> injection and no additional CO<sub>2</sub> is added during the simulation.

Figure 8. The stability of dawsonite at 60°C and 1 bar. (a) The activity of aqueous SiO<sub>2</sub> is set by equilibrium with chalcedony. Solid boundaries represent stability of dawsonite relative to albite. Dashed boundaries represent stability relative to analcime. (b) Dotted lines show analcime stability with dawsonite suppressed. Dashed ( $\log f\text{CO}_2 = -0.5$ ) boundaries and solid boundaries ( $\log f\text{CO}_2 = 1.0$ ) show the stability of dawsonite relative to albite, kaolinite and Na-beidellite (smectite). The range of  $\log f\text{CO}_2$  at Weyburn is between -0.5 and 1.0.

Figure 9. Storage of CO<sub>2</sub> in supercritical fluid, saline formation water, minerals and oil at the end of 50 years of injection at the Phase 1A area in Weyburn.



## **Acknowledgements**

The International Energy Agency Weyburn–Midale project is coordinated by the Petroleum Technology Research Center of Regina, Saskatchewan, in collaboration with Cenovus (the operator of the Weyburn oilfield) and Apache Corporation (the operator of the Midale oilfield). Financial sponsorship of the project was provided by Natural Resources Canada, the U.S. Department of Energy, Alberta Energy Research Institute, Saskatchewan Industry and Resources, the European Community and ten industrial sponsors.

We gratefully acknowledge the assistance of several individuals and organizations. Steve Whittaker, Chris Gilboy, and Erik Nickel of Saskatchewan Industry and Resources (SIR) provided help in obtaining core samples. Ian DeWolfe, (University of Calgary) assisted in sampling and sample preparation. Geoff Burrowes (Cenovus) took time to familiarize KD with typical Weyburn Unit core. Geoff Burrowes, Trevor Westman and Stan Wright (Cenovus) provided estimates of total pore volume, fluid saturations, flow unit interval information for cored wells and petrophysical data, as well as patient assistance with a range of other requests for data. Analytical assistance from Rob Marr and Mickey Horvath (U of Calgary), Pam King and Roger Mason (Memorial University of Newfoundland), is greatly appreciated. Discussion with Bill Gunter and Dirk Kirste helped to clarify the constraints on equilibrium and kinetic reaction path models. Reviewers provided insightful comments that greatly improved the final manuscript.